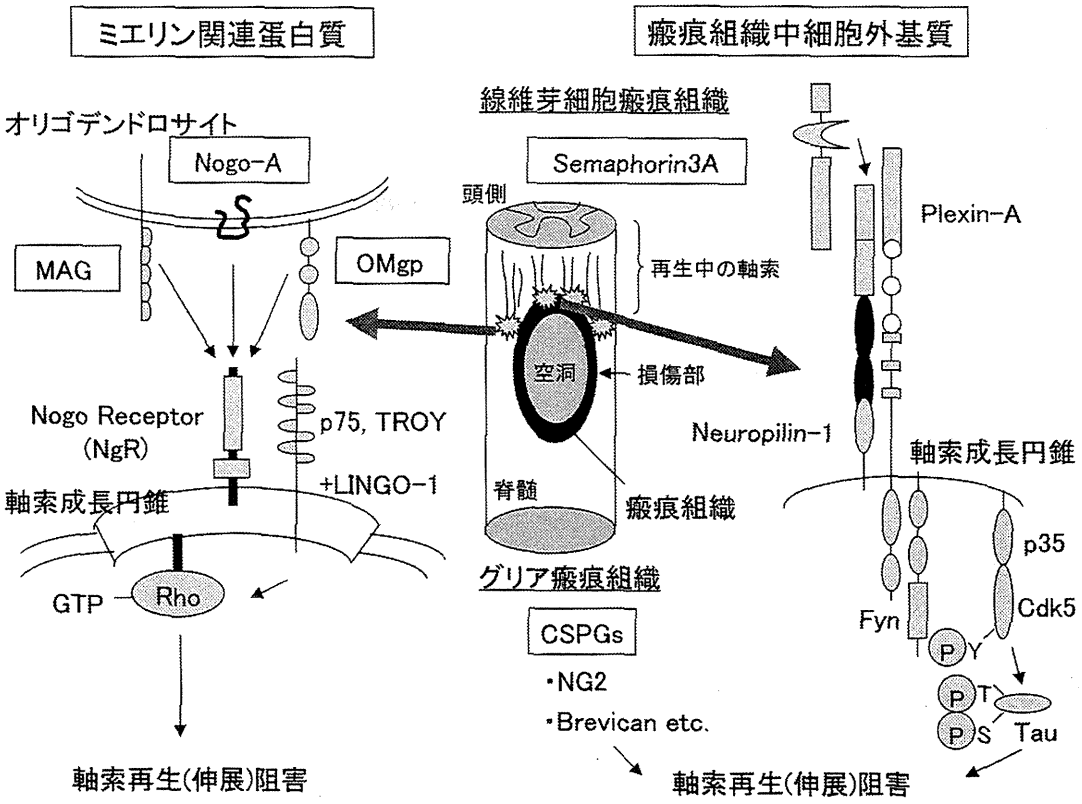

図3　中枢神経系における軸索再生（伸展）阻害因子のシグナル伝達経路
ミエリン関連蛋白質のうち Nogo-A, MAG, OMgp の3分子は，興味深い事に構造上全く異なる分子でありながら，共通のレセプター，Nogo Receptor に ligand として結合し，その co-receptor として同定された p75, TROY, LINGO-1 などを通じて，軸索再生阻害のシグナルを細胞内に伝達していく．

らを直接的に比較するような研究はこれまでには報告されていないが，それぞれの分子がそれぞれの場所で重要な役割を果たしているものと一般的には見なされており，これらを包括的にコントロールするような手段を開発する事が，臨床的にはより良い軸索再生を得るために重要な課題の1つであると考えられる．

3．ニューロンの軸索側の intrinsic な growth ability の制御機構の解明

一方，ニューロンの軸索側の intrinsic な伸長能の制御機構の解明という点においては，先程述べた DRG における conditioning lesion のシステム[1]（図2）を利用する事により，幾つかの興味深い報告が成されてきた．その1つとして，細胞内の cAMP の level を上昇させる事により，extrinsic な軸索再生阻害因子の作用を相殺する事が可能であり，また，DRG 内に *in vivo* で cAMP を注入する事により，conditioning lesion の効果[1]が mimic 可能である事などが報告されて来た[24]．また，細胞内の情報伝達路の中で，JAK2/STAT3 系の pathway が，DRG ニューロンに対して同様な効果を持つ事も報告されて来ている[25]．DRG における conditioning lesion のシステム[1]の前述したような有用性を利用して，マイクロアレイなどを用いたスクリーニングも近年は多々行われており，軸索再生を制御する intrinsic なメカニズムに関する分子生物学的解明は，様々なアプローチから進んで来ている．

今後の課題・展望

初めにも述べた如く，哺乳類の成体中枢神経系のニューロンの軸索は末梢神経系のニューロンの軸索に比して再生能に乏しいが，これらの分子生物学的制御機構を解明する事は，脊髄損傷等の中枢神経系の損傷後に，より良い軸索の再生を得るためには極めて重要な課題の1つであり，本稿では主にこれらに焦点を当てて概説して来た．当然予測出来る事ながら，extrinsic な軸索再生阻害因子の機能の減衰と intrinsic な伸長能の促進をそれぞれ得る手段を併用した際に，相加的な軸索再生が認められ

たという報告もあり，こうした異なった様々なアプローチからの軸索再生促進戦略の併用といった点も，特に臨床的観点からは重要である．また同時に，再生後の軸索の適切なる wiring の制御の問題も極めて重要な次なる課題の一つであり，これらを包括的に制御可能な手段の開発に向けて，様々なアプローチ・角度からの研究が世界各地で現在，行われている所である．

文　献

1) Neumann S, et al. : Regeneration of dorsal column fibers into and beyond the lesion site following adult spinal cord injury. Neuron 23 : 83-91, 1999
2) Chen MS, et al. : Nogo-A is a myelin-associated neurite outgrowth inhibitor and an antigen for monoclonal antibody IN-1. Nature 403 : 434-439, 2000
3) GrandPre T, et al. : Identification of the Nogo inhibitor of axon regeneration as a Reticulon protein. Nature 403 : 439-444, 2000
4) Liu BP, et al. : Myelin-associated glycoprotein as a functional ligand for the Nogo-66 receptor. Science 297 : 1190-1193, 2002
5) Domeniconi M, et al. : Myelin-associated glycoprotein interacts with the Nogo66 receptor to inhibit neurite outgrowth. Neuron 35 : 283-290, 2002
6) Wang KC, et al. : Oligodendrocyte-myelin glycoprotein is a Nogo receptor ligand that inhibits neurite outgrowth. Nature 417 : 941-944, 2002
7) Jones LL, et al. : NG2 is a major chondroitin sulfate proteoglycan produced after spinal cord injury and is expressed by macrophages and oligodendrocyte progenitors. J. Neurosci. 22 : 2792-2803, 2002
8) Pasterkamp RJ, et al. : Peripheral nerve injury fails to induce growth of lesioned ascending dorsal column axons into spinal cord scar tissue expressing the axon repellent Semaphorin3A. Eur. J. of Neurosci. 13 : 457-471, 2001
9) Winter FD, et al. : Injury-induced class 3 semaphorin expression in the rat spinal cord. Exp. Neurol. 175 : 61-75, 2002
10) Fournier AE, et al. : Identification of a receptor mediating Nogo-66 inhibition of axonal regeneration. Nature 409 : 341-346, 2001
11) Wang KC, et al. : P75 interacts with the Nogo receptor as a co-receptor for Nogo, MAG and OMgp. Nature 420 : 74-78, 2002
12) Yamashita T, et al. : The p75 receptor transduces the signal from myelin-associated glycoprotein to Rho. J. Cell Biol. 157 : 565-570, 2002
13) Yamashita T, et al. : Neurotrophin binding to the p75 receptor modulates Rho activity and axonal outgrowth. Neuron 24 : 585-593, 1999
14) Park JB, et al. : A TNF receptor family member, TROY, is a coreceptor with Nogo receptor in mediating the inhibitory activity of myelin inhibitors. Neuron 45 : 345-351, 2005
15) Shao Z, et al. : TAJ/TROY, an orphan TNF receptor family member, binds Nogo-66 receptor 1 and regulates axonal regeneration. Neuron 45 : 353-359, 2005
16) Mi S, et al. : LINGO-1 is a component of the Nogo-66 receptor/p75 signaling complex. Nat. Neurosci. 7 : 221-228, 2004
17) Zheng B, et al. : Lack of enhanced spinal regeneration in Nogo-deficient mice. Neuron 38 : 213-224, 2003
18) Simonen M, et al. : Systemic deletion of the myelin-associated outgrowth inhibitor Nogo-A improves regenerative and plastic responses after spinal cord injury. Neuron 38 : 201-211, 2003
19) Kim JE, et al. : Axon regeneration in young adult mice lacking Nogo-A/B. Neuron 38 : 187-199, 2003
20) Zheng B, et al. : Genetic deletion of the Nogo receptor does not reduce neurite inhibition in vitro or promote corticospinal tract regeneration in vivo. Proc. Natl. Acad. Sci. USA 102 : 1205-1210, 2005
21) Kim JE, et al. : Nogo-66 receptor prevents raphespinal and rubrospinal axon regeneration and limits functional recovery from spinal cord injury. Neuron 44 : 439-451, 2004
22) Bradbury EJ, et al. : Chondroitinase ABC promotes functional recovery after spinal cord injury. Nature 416 : 636-640, 2002
23) Kaneko S, et al. : A selective Sema3A inhibitor enhances regenerative responses and functional recovery of the injured spinal cord. Nat. Med. 12 : 1380-1389, 2006
24) Qiu J, et al. : Spinal axon regeneration induced by elevation of cyclic AMP. Neuron 34 : 895-903, 2002
25) Qiu J, et al. : Conditioning injury-induced spinal axon regeneration requires signal transducer and activator of transcription 3 activation. J. Neurosci. 25 : 1645-1653, 2005

Roles of ES Cell-Derived Gliogenic Neural Stem/Progenitor Cells in Functional Recovery after Spinal Cord Injury

Gentaro Kumagai[1,2,3], Yohei Okada[1,4,5], Junichi Yamane[2], Narihito Nagoshi[1,2], Kazuya Kitamura[1,2], Masahiko Mukaino[1,6], Osahiko Tsuji[1,2], Kanehiro Fujiyoshi[1,2], Hiroyuki Katoh[2], Seiji Okada[7], Shinsuke Shibata[1], Yumi Matsuzaki[1], Satoshi Toh[3], Yoshiaki Toyama[2], Masaya Nakamura[2]*, Hideyuki Okano[1]*

1 Department of Physiology, Keio University School of Medicine, Tokyo, Japan, **2** Department of Orthopedic Surgery, Keio University School of Medicine, Tokyo, Japan, **3** Department of Orthopedic Surgery, Hirosaki University Graduate School of Medicine, Hirosaki, Japan, **4** Department of Neurology, Graduate School of Medicine, Nagoya University, Nagoya, Japan, **5** Kanrinmaru Project, Keio University School of Medicine, Tokyo, Japan, **6** Department of Rehabilitation Medicine, Keio University School of Medicine, Tokyo, Japan, **7** Department of Research Super Star Program Stem Cell Unit, Graduate School of Medical Science, Kyusyu University, Fukuoka, Japan

Abstract

Transplantation of neural stem/progenitor cells (NS/PCs) following the sub-acute phase of spinal cord injury (SCI) has been shown to promote functional recovery in rodent models. However, the types of cells most effective for treating SCI have not been clarified. Taking advantage of our recently established neurosphere-based culture system of ES cell-derived NS/PCs, in which primary neurospheres (PNS) and passaged secondary neurospheres (SNS) exhibit neurogenic and gliogenic potentials, respectively, here we examined the distinct effects of transplanting neurogenic and gliogenic NS/PCs on the functional recovery of a mouse model of SCI. ES cell-derived PNS and SNS transplanted 9 days after contusive injury at the Th10 level exhibited neurogenic and gliogenic differentiation tendencies, respectively, similar to those seen *in vitro*. Interestingly, transplantation of the gliogenic SNS, but not the neurogenic PNS, promoted axonal growth, remyelination, and angiogenesis, and resulted in significant locomotor functional recovery after SCI. These findings suggest that gliogenic NS/PCs are effective for promoting the recovery from SCI, and provide essential insight into the mechanisms through which cellular transplantation leads to functional improvement after SCI.

Citation: Kumagai G, Okada Y, Yamane J, Nagoshi N, Kitamura K, et al. (2009) Roles of ES Cell-Derived Gliogenic Neural Stem/Progenitor Cells in Functional Recovery after Spinal Cord Injury. PLoS ONE 4(11): e7706. doi:10.1371/journal.pone.0007706

Editor: Kenji Hashimoto, Chiba University Center for Forensic Mental Health, Japan

Received August 18, 2009; **Accepted** October 9, 2009; **Published** November 6, 2009

Funding: This work was supported by grants from the Leading Project for Realization of Regenerative Medicine from the Ministry of Education, Culture, Sports, Science and Technology (MEXT) of Japan; Japan Science and Technology Agency (SORST); the Ministry of Health, Labor, and Welfare (to H. O.); the General Insurance Association of Japan (to M.N. and Y.T; this is not a commercial entity); Research Fellowships for Young Scientists from the Japan Society for the Promotion of Science (to Y. O.); Keio Gijuku Academic Development Funds; and by a Grant-in-aid for Global COE Program from MEXT to Keio University. The funders had no role in study design, data collection and analysis, decision to publish, or preparation of the manuscript.

Competing Interests: The authors have declared that no competing interests exist.

* E-mail: hidokano@sc.itc.keio.ac.jp (HO); masa@sc.itc.keio.ac.jp (MN)

Introduction

Because the adult central nervous system (CNS) has limited potential for regeneration, spinal cord injury (SCI) results in severe dysfunction, such as paraplegia and tetraplegia. With the aim of regenerating the injured spinal cord, various intraspinal cellular transplants have been investigated, especially in the sub-acute phase after injury. This period, between the acute and chronic phases, is marked by the minimal expression of cytokines, and is likely to be amenable to transplantation therapy [1,2,3,4,5]. Embryonic stem (ES) cells, with their indefinite replication potential, pluripotency, and genetic flexibility, have attracted great interest, and methods for inducing their neural differentiation have been extensively studied [6]. ES cell-derived neural progenitors are currently one of the most promising cell sources for cell transplantation therapy for treating SCI. Although previous studies demonstrated that the transplantation of mouse ES cell-derived embryoid bodies [7] or human ES cell-derived oligodendrocyte progenitor cells [8] promotes overall functional recovery after SCI, the types of neural progenitor cells most effective for treating sub-acute phase SCI has been uncertain.

We recently reported that a low concentration of retinoic acid (10^{-8} M: low-RA) can efficiently induce caudalized neural progenitors in embryoid bodies (EBs) [9], and we established a neurosphere-based culture system of ES cell-derived neural stem/progenitor cells (NS/PCs) from low-RA-treated EBs, with midbrain to hindbrain identities [10]. These ES cell-derived primary neurospheres (PNS) mainly exhibit neurogenic differentiation potentials, whereas passaged secondary neurospheres (SNS) are more gliogenic, corresponding to changes in CNS development, in which neurogenic NS/PCs predominate early in gestation and gliogenic NS/PCs predominate in mid-to-late gestation. Here, taking advantage of this difference between neurogenic PNS and gliogenic SNS, we transplanted PNS and SNS into the injured spinal cord, examined the differentiation and growth properties of the grafted cells, and compared their effects on angiogenesis, axonal regeneration, and functional recovery after SCI. We also examined the survival and growth of the

transplanted ES cell-derived NS/PCs using *in vivo*, live, bioluminescent imaging (BLI) to evaluate the tumorigenicity and safety of the grafted cells.

Results

Establishment of a Stable ES Cell Line Expressing CBR*luc* Luminescence and Venus Fluorescence

We first established an ES cell line that constitutively expresses the click beetle red-emitting luciferase (CBR*luc*) [11] and Venus [12] by introducing a CAG-CBR*luc*-IRES-Venus plasmid (Fig. 1**A**) into EB3 ES cells (CCV-ES cells) [13]. CCV-ES cells and their progenies were detected by both BLI [3,14,15] and fluorescence microscopy. To induce NS/PCs from ES cells and obtain PNS and SNS, we used a neurosphere-based culture system that we recently reported [10] (Fig. 1**B**), as described in Materials and Methods. More than 99% of the undifferentiated CCV-ES cells expressed Venus fluorescence by flow cytometry (Fig. 1**D and E**), and CCV-ES cell-derived PNS (CCV-PNS) and SNS (CCV-SNS) showed steady fluorescence that was detectable by fluorescence microscopy (Fig. 1**C**). Approximately 80% of the cells in the CCV-PNS and -SNS were positive for Venus by flow cytometry (Fig. 1**D and E**). bioluminescence imaging (BLI) revealed CBR*luc* expression in both CCV-PNS and –SNS, and we confirmed that the photon counts were in direct proportion to the cell numbers *in vitro* (Fig. 1**F**). We also confirmed that the CCV-ES cells could generate PNS and SNS similar to EB3-ES cells (Fig. 1**C**).

Distinct Differentiation Potentials of PNS and SNS *In Vitro*

We next examined the *in vitro* differentiation potentials of the PNS and SNS derived from EB3- and CCV-ES cells. PNS and SNS derived from EB3- and CCV-ES cells were allowed to differentiate in medium without FGF2 on poly-L-ornithine/fibronectin coated coverslips for 5 days, and then processed for immunocytochemistry. We examined the frequency of colonies consisting of βIII tubulin-positive neurons, GFAP-positive astrocytes, and/or O4-positive oligodendrocytes, and found that the EB3- and CCV-PNS colonies predominantly differentiated into neurons, although a small number of colonies contained both neurons and glia (Fig. 1**G**). In contrast, most of the EB3- and CCV-SNS colonies differentiated into both neurons and glia, including astrocytes and oligodendrocytes, or into only glial cells (Fig. 1**G**), demonstrating that the ES cell-derived PNS and SNS had distinct differentiation potentials *in vitro* (Fig. 1**H**). Moreover, EB3- and CCV-ES cell-derived neurospheres exhibited similar differentiation properties, confirming that the transgene in the ES cells had negligible effects on differentiation (Fig. 1**H**).

We also examined the SNS formation rates to determine the self-renewing ability of the ES cell-derived PNS. We cultured CCV-PNS at a low cell density (2.5×10^4 cells/ml), transferred them into 96-well plates at one neurosphere/well, dissociated the neurospheres, and cultured them again with FGF2 to form secondary neurospheres. Most of the CCV-PNS generated secondary neurospheres (79/90; 87.7%; from more than three independent experiments), confirming their ability to self-renew.

Transplanted SNS Prevented Atrophic Change and Demyelination after SCI

A contusive SCI was induced at the Th10 level of C57BL6 mice, and 5×10^5 cells of CCV-PNS or CCV-SNS, or PBS as a control, were injected into the lesion epicenter 9 days after injury. We refer to these, respectively, as the PNS, SNS, and control groups. After 6 weeks, histological analyses were performed. We first examined atrophic changes of the injured spinal cord by Hematoxylin-eosin (H–E) staining (Fig. 2**A and B**). The transverse area of the spinal cord at the lesion epicenter was significantly larger in the SNS group than in the control group, suggesting that SNS transplantation prevented atrophy of the injured spinal cord (Fig. 2**E**). Luxol Fast Blue (LFB) staining revealed significantly greater preservation of the myelinated areas in the SNS group compared with the control (both 2 and 6 weeks after injury) and PNS groups (Fig. 2**C and D**), from 1 mm rostral to 1 mm caudal to the epicenter (Fig. 2F). Notably, there was a significantly spared rim of white matter in the SNS group, even at the lesion epicenter, whereas the control group exhibited severely demyelinated white matter throughout the lesioned area (2 mm rostral and caudal to the lesion epicenter) (Fig. 2**C and D**).

Transplanted PNS and SNS survived in the injured spinal cord and did not form tumors

The photon count measured by bioluminescence imaging (BLI) quantifies only living cells, since the luciferin-CBR-luciferase reaction depends on oxygen and ATP. The successful transplantation of CCV-PNS and -SNS was confirmed immediately after transplantation using BLI, and the average signal intensity was $2.2\pm1.6\times10^5$ photons/mouse/sec in 22 transplanted mice. Images obtained weekly thereafter for 6 weeks showed that the signal intensity dropped sharply within the first week after transplantation, but remained at 20% of the initial photon count in both the PNS and SNS transplantation groups throughout the remaining period. Although the signal intensity at 1 week was significantly higher in the PNS group (62.4%) than in the SNS group (29.5%), there was no significant difference in the signal intensity between the PNS (12.6%) and SNS (18.9%) groups at 6 weeks, suggesting there was a similar number of live grafted PNS- and SNS-derived cells within the injured spinal cord 6 weeks after transplantation. Thus, similar numbers of grafted PNS and SNS cells may have survived in the injured spinal cord, although the possibility that the grafted cells proliferated differently in the two groups 1 to 6 weeks after transplantation cannot be excluded. Notably, a rapid increase in signal intensity, which would have suggested tumor formation, was not observed during this time period (Fig. 3**A and B**). Consistently, histological analysis confirmed that both the CCV-PNS- and CCV-SNS-derived Venus-positive cells survived without forming tumors (Fig. 3**C–F**). Quantitative analysis of the Venus-positive area revealed that there was no significant difference of the number of survived grafted cells between PNS and SNS groups 6 weeks after transplantation (Fig. 3**G**). Moreover, the data of BLI correlated well with Venus-positive area (Pearson's correlation coefficient: 0.759, $p=0.04$, Fig. 3**H**).

PNS and SNS Grafted onto Injured Spinal Cord Exhibited Differentiation Potentials Similar to Those Observed *In Vitro*

To examine the differentiation characteristics of CCV-PNS and -SNS grafted onto the injured spinal cord, we performed immunohistochemical analyses, and determined the proportion of cells immunopositive for each cell type-specific marker among the Venus-positive grafted cells [3]. Both the PNS- and SNS-derived cells integrated at or near the lesion epicenter and differentiated into Hu-positive neurons, GFAP-positive astrocytes, and APC-positive oligodendrocytes (Fig. 4**A–E**). The percentage of Hu/Venus double-positive neurons in the PNS group ($52.8\pm19.1\%$) was three times that in the SNS group ($16.3\pm5.2\%$) (Fig. 4**F**). In contrast, the percentage of GFAP/Venus double-positive astrocytes or APC/Venus double-positive

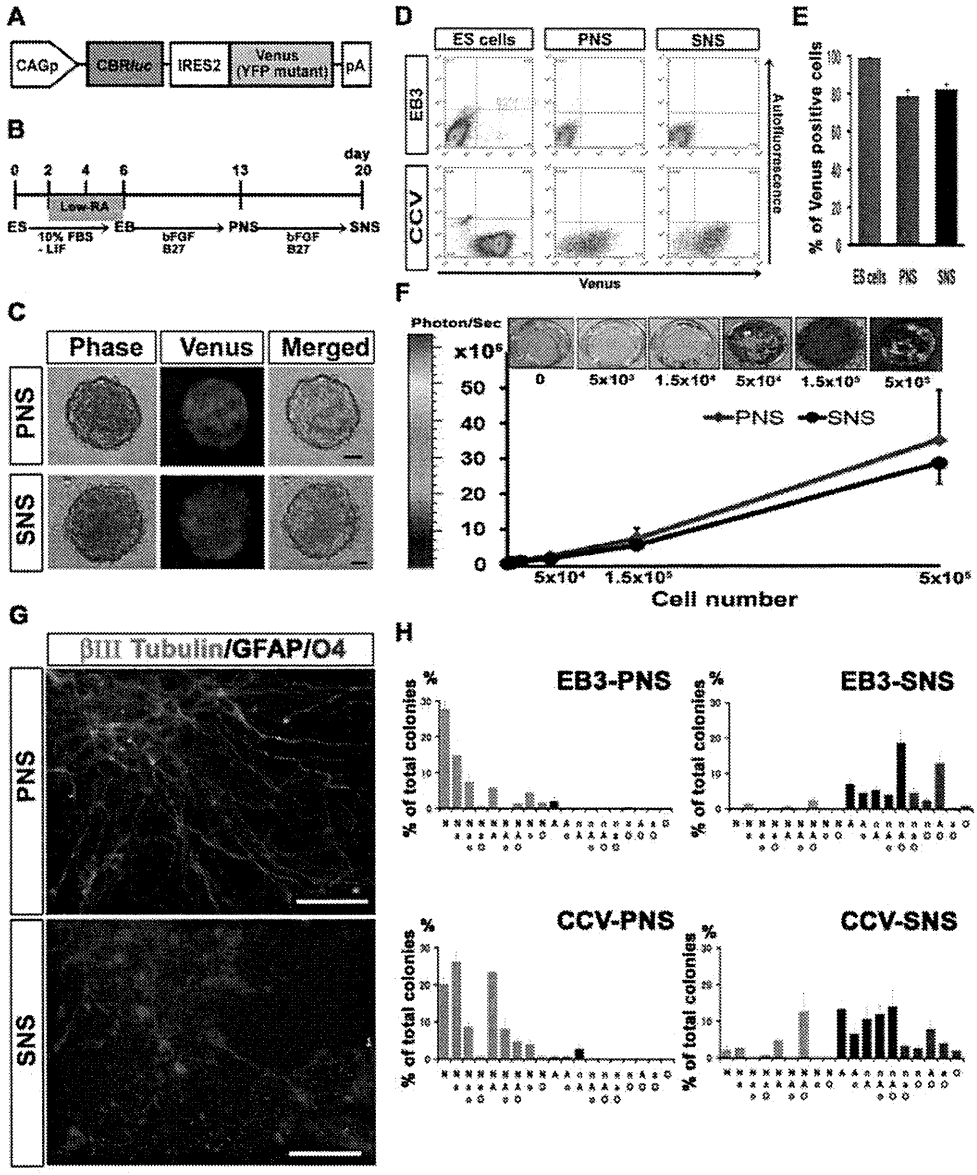

Figure 1. Establishment of a stable ES cell line expressing CBR/*luc* luminescence and Venus fluorescence, and their differentiation analysis. (A) The CAG-CBR/*luc*–IRES-Venus gene (CCV) construct. (B) Protocols for deriving neurospheres from mouse ES cells. ES cells were dissociated into single cells with 0.25% trypsin-EDTA and cultured for 6 days to allow the formation of embryoid bodies (EBs). A low concentration of RA was added on day 2 of EB formation for neural induction. The EBs were dissociated into single cells with 0.25% trypsin-EDTA and cultured in suspension for 7 days, to obtain primary neurospheres (ES cell-derived primary neurospheres, PNS). These PNS were dissociated into single cells with TripleLE Select (Invitrogen) and cultured again in suspension for 7 days under the same conditions to form secondary neurospheres (SNS). (C) Images of CCV-PNS and -SNS visualized by fluorescence microscopy. Scale bar: 100 μm. (D) Flow cytometric analysis of Venus-positive cells in PNS and SNS derived from CCV- and EB3-ES cells. (E) The proportion of Venus-positive cells among CCV-ES cells and their progenies, CCV-PNS and -SNS. Approximately 80% of the CCV-PNS and -SNS cells were positive for Venus. Values are means ± s.e.m. ($n = 3$). (F) Correlation between the cell numbers of CCV-PNS and -SNS, and the measured photon counts. BLI revealed CBR/*luc* expression in both CCV-PNS and -SNS, and we determined that the photon counts were in direct proportion to the cell numbers *in vitro*. Values are means ± s.e.m. ($n = 3$). (G)(H) Distinct differentiation potentials of PNS and SNS *in vitro*. Immunocytochemical analysis of βIII tubulin-positive neurons (N or n), GFAP-positive astrocytes (A or a), and O4-positive oligodendrocytes (O or o) (N, A, O: more than 20 cells; n, a, o: fewer than 19 cells in each colony, respectively). A neuron-only colony (N) and a colony consisting of astrocytes and oligodendrocytes (AO) are shown (G). Scale bar: 50 μm. Quantitative analysis of the *in vitro* differentiation potential of EB3-PNS and -SNS and CCV-PNS and -SNS, shown as the percentage of each phenotypic colony among the total colonies (H). The PNS colonies dominantly differentiated into neurons, while a small number of colonies contained glial cells. On the other hand, most of the SNS colonies differentiated into both neurons and glial cells, including astrocytes and oligodendrocytes, or into only glial cells. Values are means ± s.e.m. ($n = 3$).
doi:10.1371/journal.pone.0007706.g001

oligodendrocytes in the SNS group (42.2±14.4, 33.6±5.4%) was twice that in the PNS group (19.0±9.3, 14.8±7.1%) (Fig. 4**F**) (n = 4). The differentiation patterns of the grafted PNS and SNS were consistent with the results of the *in vitro* differentiation assay, suggesting that PNS and SNS preserved their differentiation tendencies *in vivo*.

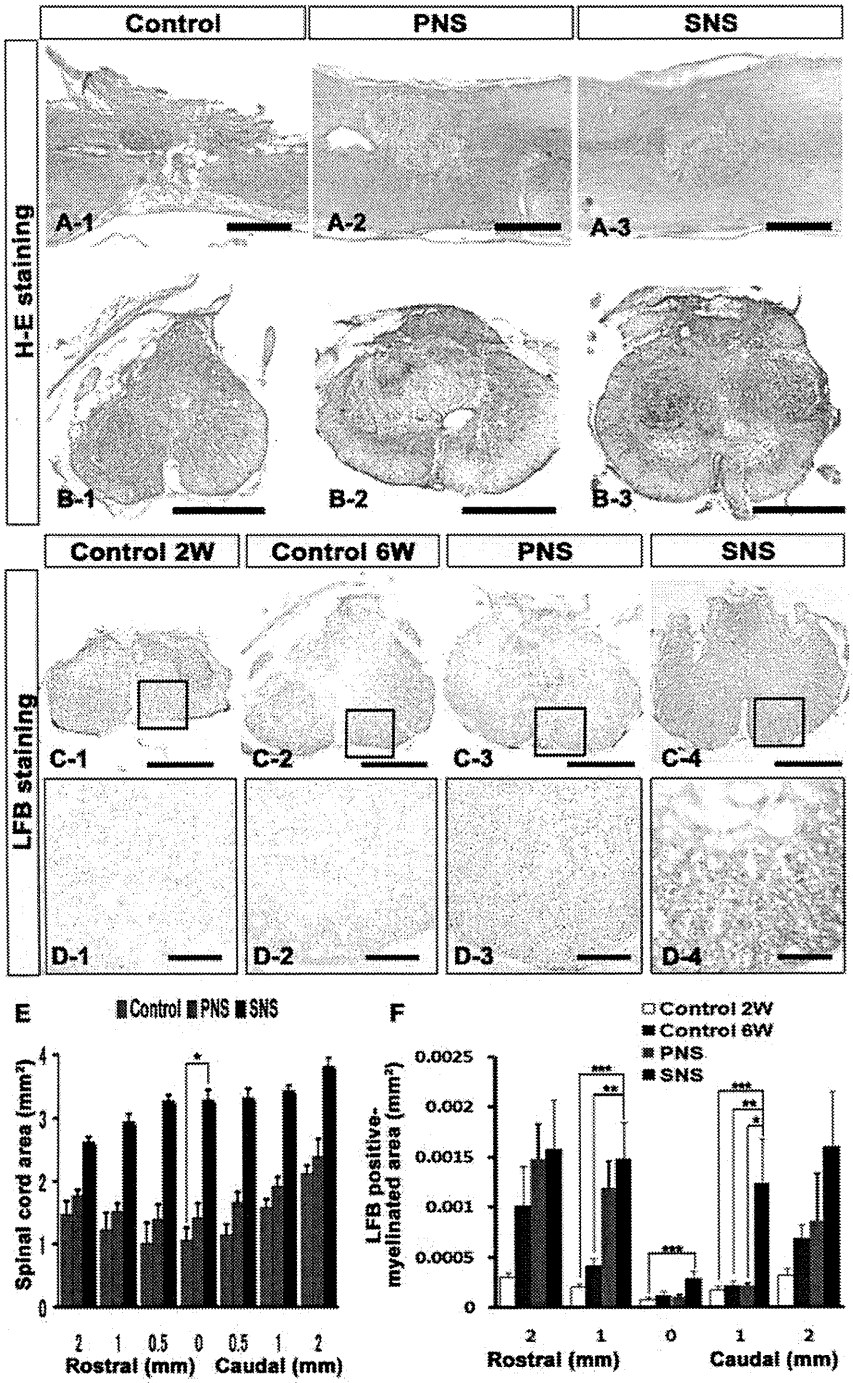

Figure 2. Transplanted SNS prevented atrophic change and demyelination after SCI. (A)(B) Representative H–E staining images of the sagittally sectioned (A1–3) and axially sectioned (B1–3) spinal cord at the lesion epicenter 6 weeks after injury. Scale bar: 500 μm. (C) Representative LFB staining images of the axially sectioned spinal cord 1 mm caudal to the lesion from each animal (2 weeks or 6 weeks after SCI for the vehicle-control group and 6 weeks after SCI for the PNS and SNS groups). Scale bar: 500 μm. (D) Higher magnification images of the boxed areas in C. Scale bar: 100 μm. (E) Quantitative analysis of the spinal cord area measured in H–E-stained axial sections through different regions. The transverse area of the spinal cord at the lesion epicenter was significantly larger in the SNS group compared with the control group. Values are means ± s.e.m. ($n = 5$). *: $P<0.05$, Control vs. SNS. (F) Quantitative analysis of the myelinated area by LFB-stained axial sections at different regions. LFB staining revealed greater preservation of myelination in the SNS group, with significant differences observed at the sites 1 mm rostral and 1 mm caudal to the epicenter compared with the control 2 or 6 weeks groups, 1 mm caudal to the epicenter compared with the PNS group, and at the epicenter compared with the control 2-week group. Values are means ± s.e.m. ($n = 5$). *: $P<0.05$, PNS vs. SNS. **: $P<0.05$, Control 6 weeks vs. SNS. ***: $P<0.05$, Control 2 weeks vs. SNS.
doi:10.1371/journal.pone.0007706.g002

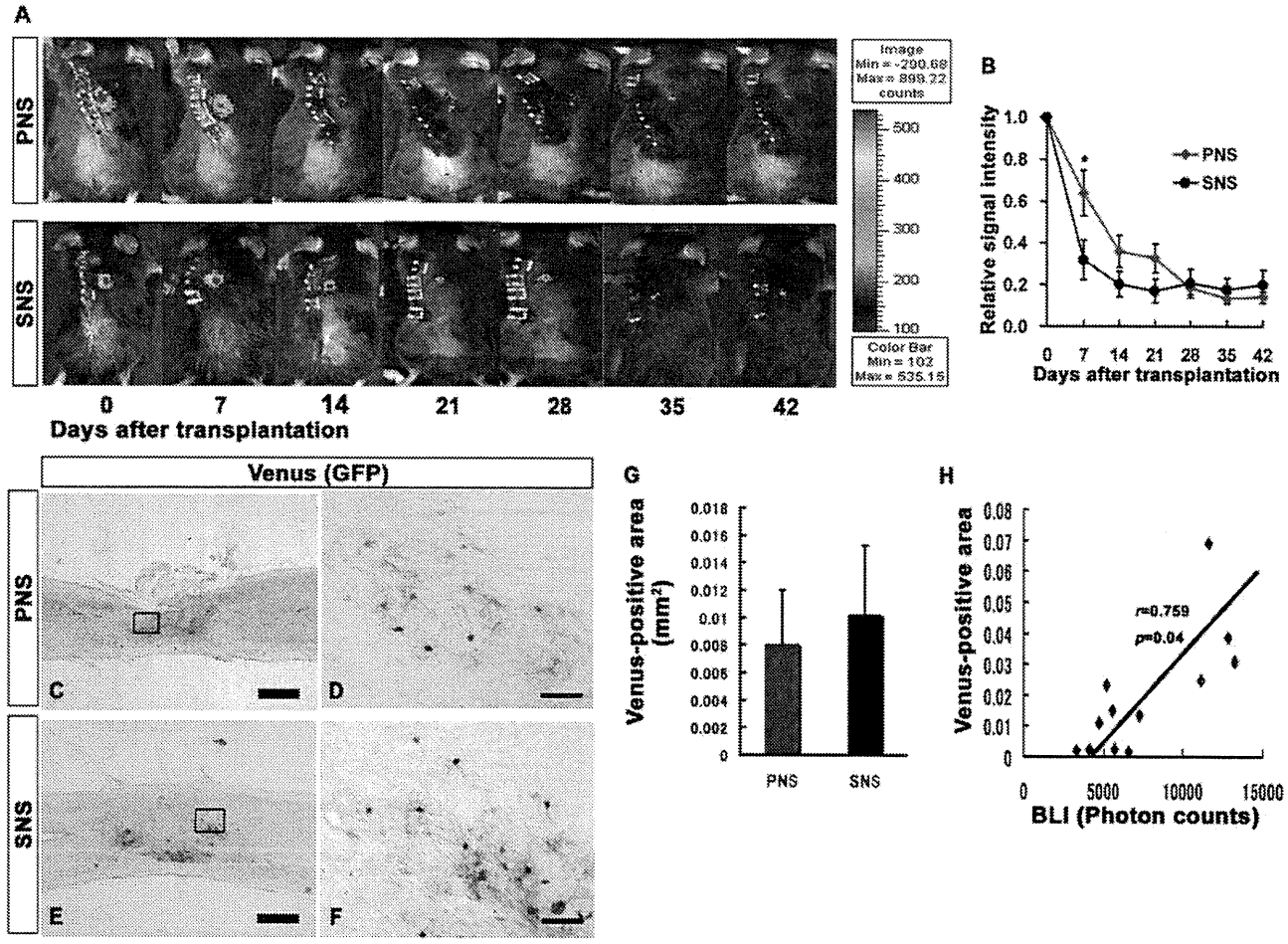

Figure 3. Transplanted PNS and SNS survived in the injured spinal cord and did not form tumors. (A) Representative BLI images of mice that received transplants of CCV-PNS and -SNS. (B) Signal intensity over time after transplantation in the PNS and SNS groups, shown relative to the initial value. Although the signal intensity at 1 week after the injury was significantly higher in the PNS group (62.4%) than the SNS group (29.5%), there was no significant difference in the signal intensity between the PNS (12.6%) and SNS (18.9%) groups 6 weeks after the injury. Values are means ± s.e.m. ($n = 11$). *: $P<0.05$, PNS vs. SNS. Scale bar: 500 μm. (C)(D)(E)(F) Representative images of sagittal sections of spinal cords grafted with PNS and SNS, which were immunostained for Venus (grafted cells) using an anti-GFP antibody. High-magnification images of the boxed areas in C and E are shown in D and F. Scale bar: 500 μm for C and E, 100 μm for D and F. Histological analysis confirmed that both PNS- and SNS-derived cells survived without forming tumors. (G) Quantitative analysis of Venus (GFP)-positive area at the lesion epicenter in midsagittal sections. Venus immunostaining revealed there was no significant difference between PNS and SNS groups 6 weeks after transplantation Values are means ± s.e.m. (n = 6). (H) Correlation of the results of BLI analysis and the quantification of Venus-positive area. The data of BLI correlated well with Venus-positive area (n = 12).

doi:10.1371/journal.pone.0007706.g003

Transplanted SNS, but Not PNS, Enhanced Angiogenesis after SCI

To examine the effects of CCV-PNS and -SNS transplantation on angiogenesis after SCI, sagittal and axial sections of the injured spinal cord were examined immunohistochemically for αSMA (a marker for smooth muscle cells) or PECAM-1 (a marker for endothelial cells). While a few αSMA-positive cells were observed at and near the lesion site in sagittal sections of both the control and PNS groups, significantly more αSMA-positive cells were found in the SNS group (Fig. 5**A and B**). These αSMA-positive cells accumulated near Venus-positive grafted cells (Fig. 5**C and D**). Similarly, significantly more PECAM-1-positive blood vessels were observed at the lesion site in the SNS group than in the PNS and control groups (Fig. 5**E–J, Y**). To clarify the underlying angiogenic signals, we examined the expression of an angiogenic growth factor, vascular endothelial growth factor (VEGF), in the grafted spinal cord by immunohistochemistry. Although a VEGF-positive area was observed at the lesion epicenter in all three groups 6 weeks after injury (Fig. 5**K–M**), it was significantly broader in the SNS group than in the other groups (Fig. 5**Z**). Furthermore, we found many GFAP/VEGF double-positive host astrocytes, which were negative for Venus (GFP) (Fig. 5**N–Q**), and a few Venus (GFP)/GFAP-positive graft-derived astrocytes expressing VEGF (Fig. 5**R–X**).

Transplanted SNS, but Not PNS, Promoted Axonal Regrowth and Enhanced Functional Recovery

To examine the effects of CCV-PNS and -SNS transplantation on axonal regrowth after SCI, we performed immunohistochemical analyses of the injured spinal cord for NF-H (RT97), 5-hydroxytryptamine (5-HT), and growth-associated protein-43 (GAP43). While few NF-H-positive axons were observed at the

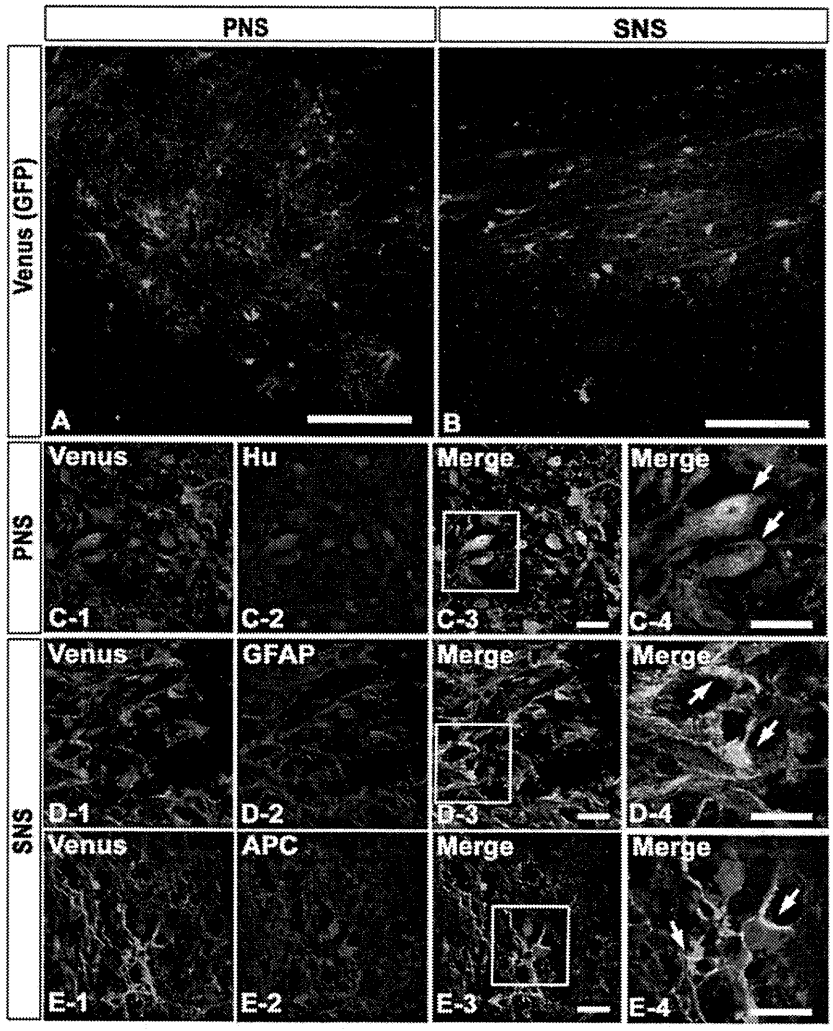

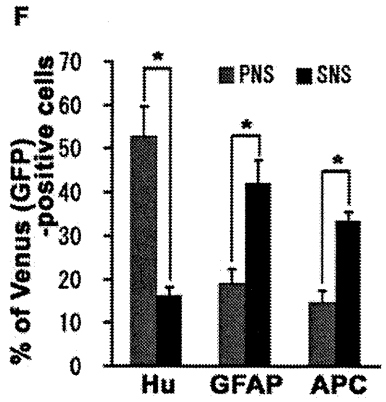

Figure 4. *In vivo* differentiation characteristics of PNS and SNS grafted onto the injured spinal cord. (A)(B) Venus-positive PNS- and SNS-derived grafted cells integrated at or near the lesion epicenter. Venus expression was detected by immunohistochemistry using an antibody against GFP. Scale bar 100 μm. (C)(D)(E) Representative immunohistochemical images of Venus-positive grafted cells that were positive for markers of neural lineages: Hu-positive neurons from PNS group (C), GFAP-positive astrocytes from SNS group (D), and APC-positive oligodendrocytes from SNS group (E). Scale bar: 20 μm. (C-4, D-4, E-4) Higher-magnification image of the boxed areas in C-3, D-3, E-3. Scale bar: 20 μm. (F) The percentage of cell type-specific marker positive cells among the Venus-positive grafted cells, showing the *in vivo* differentiation characteristics of PNS and SNS. The percentage of Hu-positive neurons in the PNS group (52.8±19.1%) was three times that in the SNS group (16.3±5.2%). In contrast, the percentage of GFAP-positive astrocytes or APC-positive oligodendrocytes in the SNS group (42.2±14.4, 33.6±5.4%) was twice that in the PNS group (19.0±9.3, 14.8±7.1%). Values are means ± s.e.m. ($n=4$). *: $P<0.05$, PNS vs. SNS.
doi:10.1371/journal.pone.0007706.g004

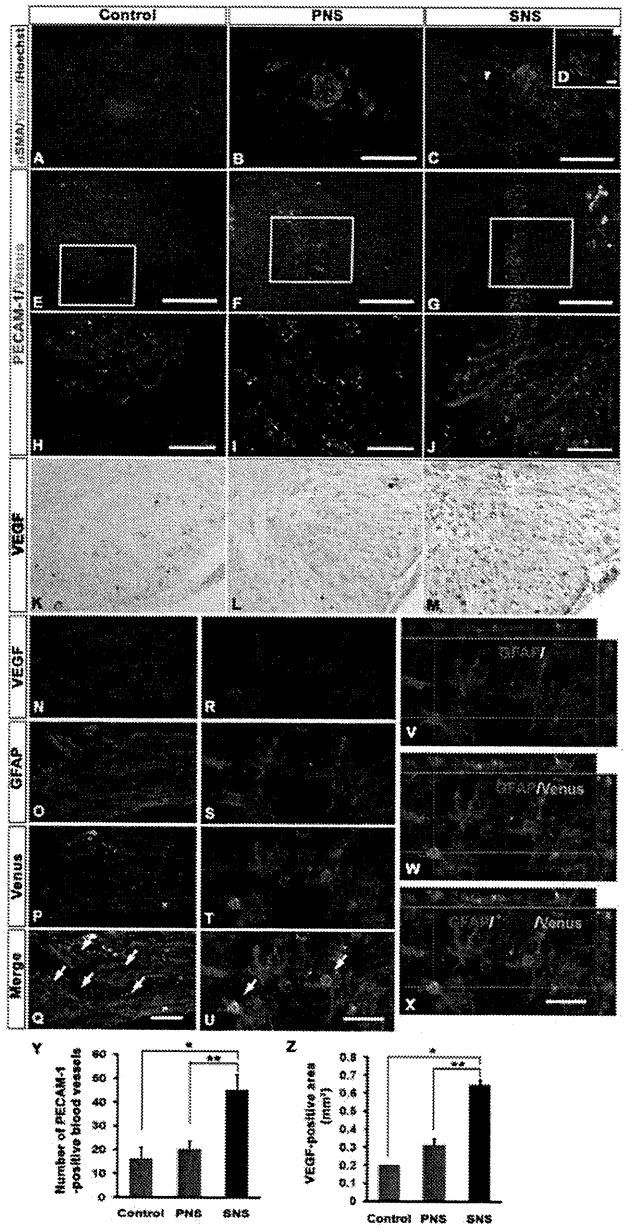

Figure 5. Transplanted SNS, but not PNS, enhanced angiogenesis after SCI. (A)(B)(C) Representative images of αSMA-immunostained sections obtained from the control (A), PNS (B), and SNS (C) groups. Scale bar: 500 μm. (D) Higher-magnification image of the area indicated by the arrowhead in C. Scale bar: 20 μm. While a few αSMA-positive Venus-expressing grafted cells were observed at and near the lesion site in sagittal sections of both the control and PNS groups, significantly more αSMA-positive cells were found in the SNS group, with Venus-positive grafted cells accumulated near the αSMA-positive cells, not colocalized with them. (E)(F)(G) Representative images of PECAM-1-immunostained sections obtained from the Control (E), PNS (F), and SNS (G) groups. Scale bar: 200 μm. (H)(I)(J) Higher-magnification images of the boxed areas in E, F, and G. Scale bar: 100 μm. (K)(L)(M) Representative images of axial sections stained for vascular endothelial growth factor (VEGF). Scale bar: 100 μm. (N–X) Expression of VEGF in GFAP-positive astrocytes among host-derived cells (N–Q) and Venus-positive (GFP immunostained) graft-derived cells (R–X) in the spinal cord from the SNS group (arrows indicate VEGF/GFAP double-positive cells). SNS transplants promoted VEGF expression in both the host- and graft-derived GFAP-positive astrocytes. Scale bar: 20 μm. (Y) Quantitative analysis of blood vessels at the lesion epicenter. PECAM-1 immunostaining revealed similar results, with significantly more PECAM-1-positive blood vessels observed at the lesion site in the SNS group compared with the PNS and control groups. Values are means ± s.e.m. (n = 3).*: P<0.05, Control vs. SNS. **: P<0.05, PNS vs. SNS. (Z) Quantitative analysis of the VEGF-positive area at the lesion epicenter. The VEGF-positive area at the lesion epicenter was significantly broader in the SNS group than in the other groups. Values are means ± s.e.m. (n = 3).*: P<0.05, Control vs. SNS. **: P<0.05, PNS vs. SNS.

doi:10.1371/journal.pone.0007706.g005

rim of the lesion epicenter in the control and PNS groups, there were significantly more NF-H-positive neuronal fibers in the SNS group at the lesion epicenter and perilesional area (Fig. 6**A, B, and E**). 5-HT-positive serotonergic fibers, which are descending raphespinal tract axons [16,17], were observed at the sites caudal to the lesion epicenter in all three groups 6 weeks after injury (Fig. 6**C**). Quantitative analysis revealed that there were significantly more 5-HT-positive fibers at the site 4 mm caudal to the lesion epicenter (Th10 level), which was approximately at the L1 level, in the SNS group compared with the other groups (Fig. 6F).

While few GAP43-positive axons [18,19,20] were detected caudal to the lesion epicenter in the control and PNS groups, there were significantly more GAP43-positive fibers in the SNS group in the ventral region 1 mm caudal to the lesion epicenter (Fig. 6**D, G**), suggesting that transplantation of the gliogenic SNS, but not of the neurogenic PNS, promoted axonal regeneration in the injured spinal cord.

We also observed NF-H-positive neuronal fibers extending along with the GFAP-positive immature astrocytes, which may have been partially derived from the grafted Venus-positive cells, and crossing the perilesional area in the SNS group (Fig. 7**A and B**). Furthermore, the SNS-derived Venus-positive cells differentiated into MBP-positive oligodendrocytes, which myelinated NF-H-positive fibers (Fig. 7**C**). Electron microscopy also revealed active remyelination in the SNS group (Fig. 7**D–F**). The grafted cells were in small groups containing 50–100 cells (Fig. 7**D**). The axons at these sites were enwrapped by myelin sheathes of various thicknesses and numbers of lamellae, which were contributed by the grafted cells, as confirmed by immunolabeling with an anti-GFP antibody to distinguish the transplanted cells from the locally surviving recipient cells (Fig. 7**E**). A much higher magnification revealed nanogold-labeled Venus-positive spots in the outer and inner mesaxons of the myelin cytoplasm. Some axons close to the lesion epicenter had undergone considerable re-myelination, and were enwrapped in spirals of more than ten layers of compacted lamellae (Fig. 7**F**).

Finally, we monitored the locomotor functional recovery in all three groups using the BMS scoring scale [21]. The contusive SCI resulted in complete paralysis (BMS score 0) on day 1, followed by gradual recovery with a plateau around 3 weeks. Although there was no significant difference in the BMS scores among the control, PNS, and SNS groups on day 14, the SNS group exhibited significantly better functional recovery than the PNS and control groups on day 21 and thereafter. On the other hand, there was no significant difference in the BMS scores between the PNS and control groups (Fig. 7**G**). From a clinical perspective, the recovery of the SNS group to levels exhibiting frequent to consistent weight-supported plantar steps and occasional forelimb-hindlimb coordination was especially noteworthy.

Discussion

Methods for effectively inducing neural differentiation from pluripotent ES cells have been extensively studied [6] and are

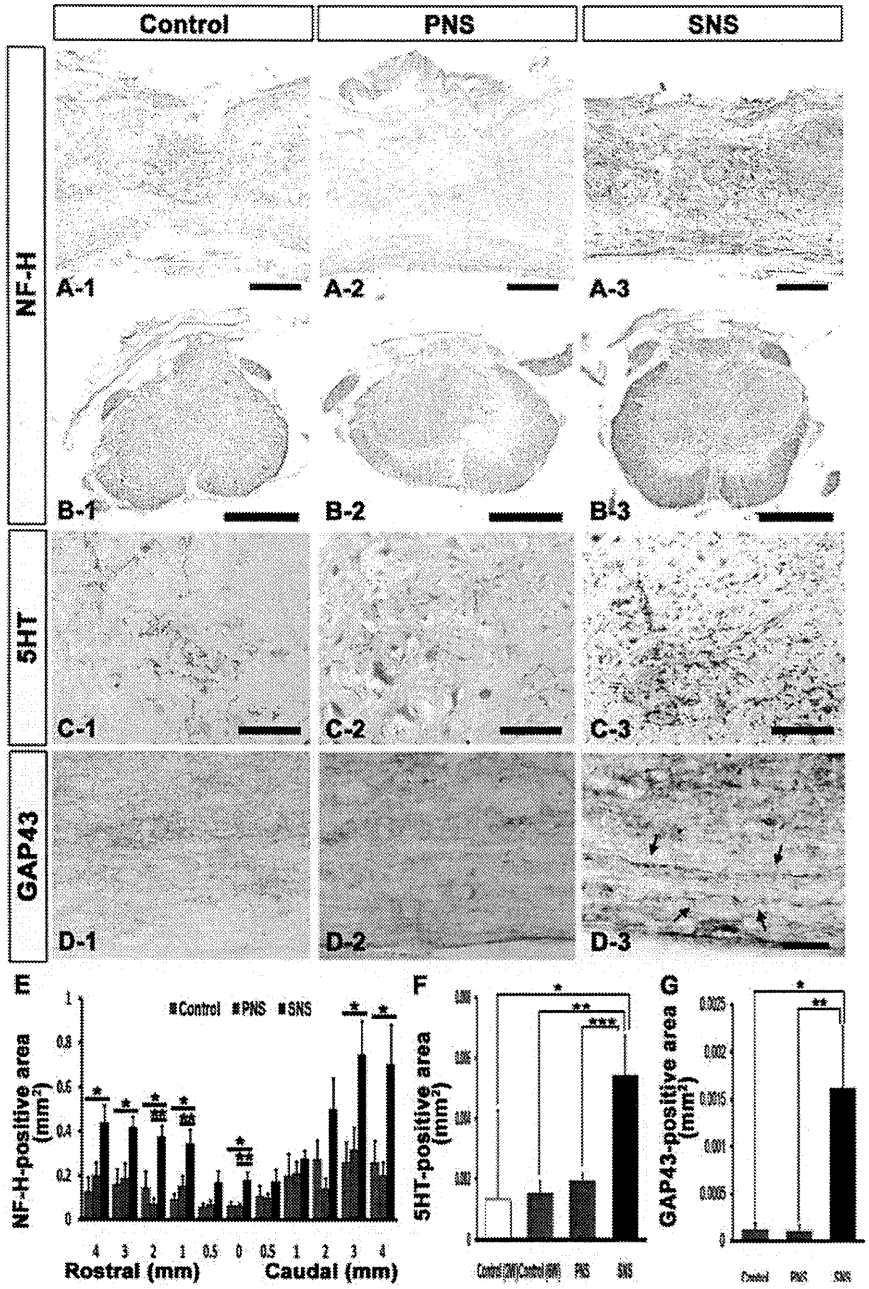

Figure 6. Transplanted SNS, but not PNS, promoted axonal growth. (A) Representative images of sagittal sections stained for NF-H in all three groups. Scale bar: 200 μm. (B) Representative images of axial sections stained for NF-H at the lesion epicenter in all three groups. Scale bar: 500 μm. (C) Representative images of axial sections stained for 5-HT 4 mm caudal to the epicenter from all three groups. Scale bar: 100 μm. (D) Representative images of midsagittal sections stained for GAP43 in the ventral region 1 mm caudal to the epicenter from all three groups, and intact spinal cord. Arrows: GAP43-positive fibers. Scale bar: 50 μm. (E) Quantitative analysis of the NF-H-positive area at each distance point. While few NF-H-positive neuronal fibers were observed at the rim of the lesion epicenter in both the control and PNS groups, there were significantly more NF-H-positive neuronal fibers in the SNS group (B-3) at the lesion epicenter, 1, 2, 3, 4 mm rostral and 3, 4 mm caudal to the lesion epicenter compared with the control group (B-1), and at the lesion epicenter and 1, 2 mm rostral to the lesion site compared with the PNS group (B-2). Values are means ± s.e.m. ($n=5$). *: $P<0.05$, Control vs. SNS. **: $P<0.05$, PNS vs. SNS. (F) Quantitative analysis of the 5-HT-positive area in axial sections 4 mm caudal to the lesion epicenter. Significantly more 5-HT-positive fibers were observed in the SNS group compared with the other groups. Values are means ± s.e.m. ($n=3$).*: $P<0.05$, Control (2 weeks after injury) vs. SNS. **: $P<0.05$, Control (6 weeks after injury) vs. SNS. ***: $P<0.05$, PNS vs. SNS. (G) Quantitative analysis of the GAP43-positive area in midsagittal sections in the ventral region 1 mm caudal to the epicenter. Significantly more GAP43-positive fibers were observed in the SNS group than in the other groups. Values are means ± s.e.m. ($n=4$). *: $P<0.05$, Control vs. SNS. **: $P<0.05$, PNS vs. SNS.

doi:10.1371/journal.pone.0007706.g006

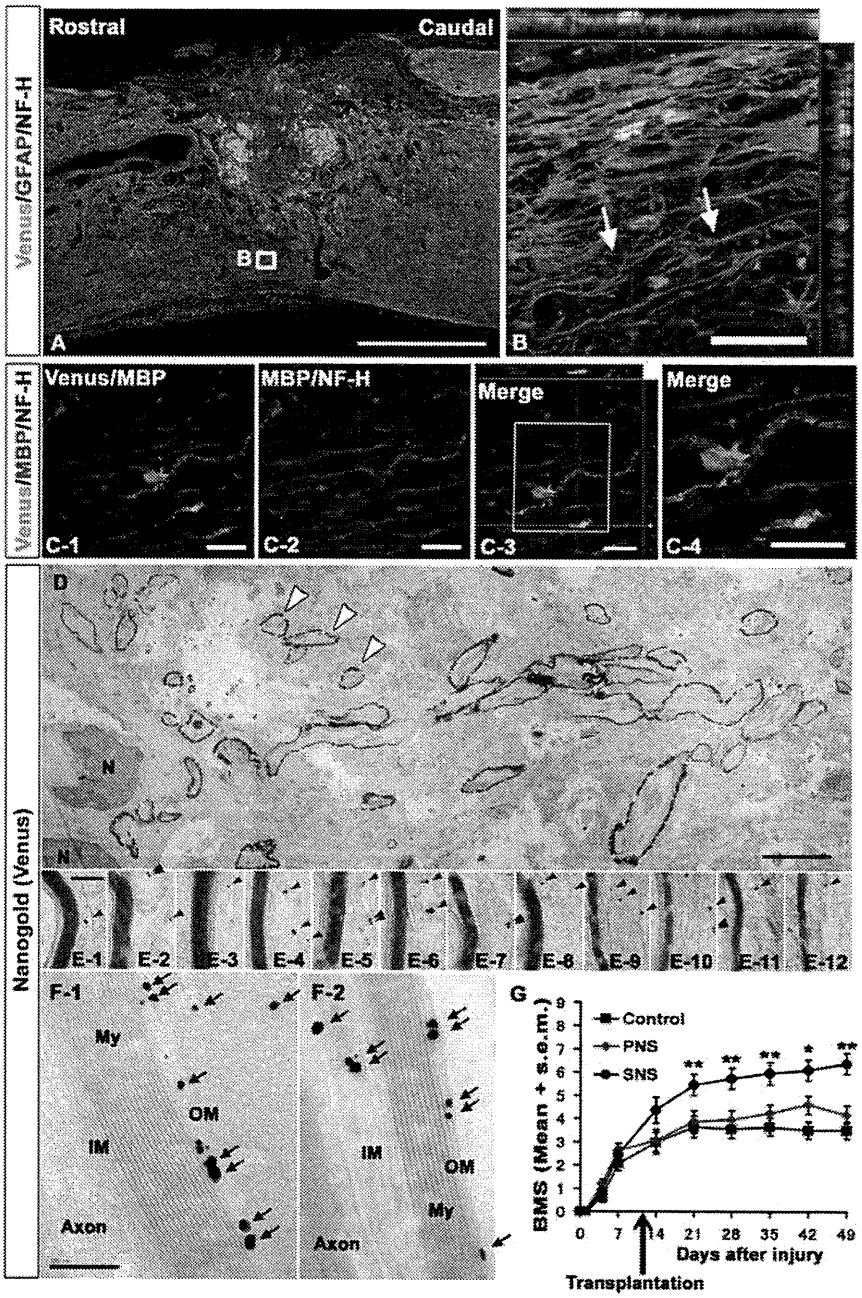

Figure 7. Transplanted SNS, but not PNS, promoted axonal growth, remyelination and functional recovery. (A) NF-H-positive neuronal fibers were observed along with GFAP-positive immature astrocytes derived either from the Venus-positive grafts or the host, and crossed the perilesional area in the SNS group. Scale bar: 50 μm. (B) Higher magnification images of the boxed area in A. Arrows: some examples of axons associated with Venus (GFP)-positive astrocytes. (C) Immunohistochemical analysis of MBP and NF-H in the SNS-transplanted injured spinal cord. SNS-derived Venus-positive cells differentiated into MBP-positive oligodendrocytes, which myelinated NF-H-positive fibers. Scale bar: 20 μm. (D)(E)(F) Representative electron-microscopic images of a remyelination site in sagittal sections from injured spinal cords grafted with SNS, which were immunostained for Venus (grafted cells) using an anti-GFP antibody. Low-magnification images show a group of grafted cells with active remyelination (some indicated by open arrowheads) (D). High-magnification images from (E-1) to (E-12) were obtained from (D), and show various numbers of lamellae in the myelin sheath. The remyelinating transplanted cells were detected as black dots (arrowheads). Venus (GFP)-positive dots (arrows) were localized to the outer and inner mesaxons of the myelin cytoplasm (OM, IM) (F). My: Myelination, N: Nucleus, Scale bar: 5 μm for D, 200 nm for E and F. (G) Mean Basso Mouse Scale for Locomotion (BMS) scores for each group over the 49-day recovery period. Although there was no significant difference in the BMS scores among the control, PNS, and SNS groups on day 14, the SNS group exhibited significantly better functional recovery than the PNS and control groups on day 21 and thereafter. On the other hand, there was no significant difference in the BMS scores between the PNS and control groups. Values are means ± s.e.m. ($n=11$), *: $P<0.05$, SNS vs. control, 42 days after injury. **: SNS vs. PNS or SNS vs. control on day 21, 28, 35, and 49 after injury.

doi:10.1371/journal.pone.0007706.g007

expected to be applied in cell replacement therapies for SCI [22]. However, detailed investigations of the optimal cell sources for promoting recovery from SCI are lacking. We recently developed an ES cell culture system that recapitulates the temporal progression of NS/PCs from the FGF-responsive early neurogenic NS/PCs to the EGF-responsive late gliogenic NS/PCs, consistent with CNS development *in vivo* [10,23] (Fig. 1**G, H**). Taking advantage of this difference in differentiation tendency, here we examined the distinct effects of the neurogenic PNS and gliogenic SNS on recovery following SCI.

One of the mechanisms underlying this developmental stage-dependent gliogenic transition of NS/PCs is the epigenetic regulation of glial cell-specific genes. The gradual demethylation of CpGs around the Stat3 recognition sequence in the GFAP promoter is thought to be involved in the developmental stage-dependent increase in transcription of the GFAP gene and the acquisition of astrocytic differentiation potentials [24,25,26]. Interestingly, this process is also observed in our ES cell-derived neurosphere system, in which the proportion of unmethylated CpGs in this region gradually increases during the development of ES cells into secondary neurospheres [10]. This may explain why the *in vitro* differentiation potentials of both the PNS and SNS were preserved even after their transplantation into injured spinal cord, despite its gliogenic environment (Fig. 4**A–F**) [27]. Since there was no significant difference in the numbers of grafted PNS and SNS in the injured spinal cord 6 weeks after transplantation, the difference in the in vivo differentiation potentials of the grafted neurospheres was the critical factor influencing the functional recovery after SCI. More than 70% of the grafted SNS cells differentiated into GFAP-positive astrocytes or APC-positive oligodendrocytes, and the engraftment of these cells led to improved functional recovery (Fig. 4**F**). In contrast, engrafted PNS cells, which mainly differentiated into neurons, did not promote functional recovery.

Determining the exact mechanisms through which the transplanted SNS, or glial cells, improved the recovery of the traumatically injured CNS has been challenging. The engrafted SNS cells could promote a wide range of effects, and here we showed positive effects of their transplantation on tissue sparing, myelination, angiogenesis, and axonal regeneration compared with the control group, and on myelination, angiogenesis, and axonal regeneration compared with the PNS group. One possible explanation for the functional recovery observed in the SNS group is that the SNS-derived astrocytes provided axonal guidance cues. This idea is supported by previous studies in which glial progenitors or glial progenitor-derived astrocytes were engrafted [28,29,30,31]. Immature astrocytes purified from the postnatal CNS have been shown to promote extensive neurite growth from a variety of neurons [32,33].

Although the reactive astrocytes in glial scar tissue express proteoglycans that can inhibit axonal growth, and have been shown to play a major role in the formation of misaligned scar tissue at sites of injury [34,35,36,37,38], we and others have previously shown that reactive astrocytes also have pivotal roles in the repair of injured tissue and recovery of motor function in the subacute phase after SCI, by sealing off injured areas and preventing the further spread of damage. They also produce an array of neurotrophic and growth factors [39]. Moreover, some astrocytes in the host spinal cord acquire stem-cell properties after injury and hence represent a promising cell type for initiating repair [40]. In combination with host astrocytes, immature astrocytes generated by the grafted SNS may express axonal growth-supporting molecules such as laminin, fibronectin, nerve growth factor (NGF), neurotrophin-3 (NT-3), vasoactive intestinal polypeptide (VIP), and activity-dependent neurotrophic factor (ADNF) [41] with minimal expression of chondroitin sulfate proteoglycans (CSPGs) [42]. In addition, SNS transplantation 9 days after SCI, between the acute and chronic phases, is likely to prevent grafted cells from differentiating into glial scar-forming reactive astrocytes due to their minimal expression of cytokines [3,43] and instead generate immature astrocytes, which provide cues for axonal regeneration. In fact, our immunohistochemical analysis revealed NF-H-positive neuronal fibers aligned with GFAP-positive fibers within the lesion site of the SNS group, suggesting that the SNS transplants promoted the alignment of regenerating axons with the fibers of astrocytes, which in turn promoted axonal growth into and out of the SNS grafts (Fig. 7**A and B**). In addition, the 5-HT-raphespinal system of the spinal cord has been shown to represent axonal regeneration after spinal cord injury [16,17], and the apparent regeneration and/or sparing of host 5-HT-positive fibers elicited by the grafting of SNS may have contributed to the observed functional recovery, since these fibers were not observed in the control or PNS groups (Fig. 6**C and F**).

Another possible explanation for the functional improvement in the SNS group is the enhancement of angiogenesis, since angiogenesis is reported to promote endogenous repair and support axonal outgrowth after SCI [44]. Under hypoxic conditions, astrocytes express angiogenic growth factors, including VEGF [45,46]. We revealed that transplanted SNS, but not PNS, enhanced angiogenesis after SCI (Fig. 5**A–Z**). We observed many host astrocytes (Fig. 5**N–Q**), and a few SNS-graft-derived astrocytes that expressed VEGF (Fig. 5**R–X**), suggesting that the SNS transplants promoted VEGF expression in both the host- and graft-derived GFAP-positive astrocytes. The increase in blood vessels elicited by the transplantation of ES cell-derived gliogenic NS/PCs may have improved axonal growth and prevented atrophy of the injured spinal cord.

The functional improvement might also be due to remyelination by SNS-derived oligodendrocytes, as supported by previous transplantation studies of ES cell-derived NS/PCs or oligodendrocyte progenitor cells (OPCs) [8,47]. While the neurogenic PNS dominantly differentiated into Hu-positive neurons (Fig. 4**F**), the gliogenic SNS differentiated into APC-positive oligodendrocytes that provided MBP-positive sheathes and promoted myelination after SCI (Fig. 2**C, D, F**, and Fig.7**C–F**).

In summary, here we took advantage of our recently established neurosphere-based culture system of ES cell-derived NS/PCs, in which PNS and SNS exhibit neurogenic and gliogenic potentials, respectively, and found that SNS cells were the most effective for promoting recovery after SCI. We showed that grafted SNS generated approximately equal numbers of GFAP-positive astrocytes and APC-positive oligodendrocytes in vivo. Both of these glial cell types may have contributed to the functional recovery, through trophic effects and the promotion of angiogenesis and axonal regeneration by immature astrocytes, and possibly through remyelination by grafted oligodendrocyte progenitor cells. Notably, the transplantation of PNS did not improve the functional recovery after SCI. These findings provide critical information for clinical trials using human ES- and induced pluripotent stem cell (iPS)-derived NS/PC transplantation for SCI.

Moreover, our results suggest that ES cell-derived NS/PCs cultured for relatively long periods may provide sufficient amounts of efficient glial donor cells for cell transplantation therapies. This strategy may also prevent the contamination of tumorigenic undifferentiated ES cells that occurs during long-term culture under serum-free conditions, and support the development of safe embryonic stem cell-based treatment strategies for spinal cord

injury. Although both the CCV-PNS- and CCV-SNS-derived Venus-positive cells survived without forming tumors for 6 weeks after transplantation in this study, careful observation for a longer period will be necessary to assess the possibility of tumor formation.

In the near future, other types of pluripotent stem cells, such as nuclear transfer ES (ntES) and iPS cells, which avoid the risk of immunological rejection and ethical concerns, will need to be evaluated to examine the applicability of human ES cells and human iPS cells in clinical applications.

Materials and Methods

ES Cell Culture and Differentiation

Mouse ES cells (EB3) [13] grown on gelatin-coated (0.1%) tissue-culture dishes were maintained in standard ES cell medium and used for EB formation as previously described, with slight modifications [9,13,48]. For neural induction, ES cells were dissociated into single cells with 0.25% trypsin-EDTA and cultured in bacteriological dishes for 6 days, to allow the formation of EBs. A low concentration of RA (low-RA; 10^{-8} M, Sigma) was added on day 2 of EB formation. The EBs were dissociated into single cells with 0.25% trypsin-EDTA and cultured in suspension at 5×10^4 cells/ml for 7 days in Media hormone mix (MHM) medium with 20 ng/ml FGF2 (Peprotech) and 2% B27 (Invitrogen), to obtain primary neurospheres (PNS). These PNS were dissociated into single cells with TripleLE Select (Invitrogen) and cultured again in suspension at 5×10^4 cells/ml for 7 days under the same conditions, to form secondary neurospheres (SNS) (Fig. 1**B**) [10]. For differentiation analysis, PNS and SNS were allowed to differentiate on poly-L-ornithine/fibronectin-coated coverslips for 5 days, followed by immunocytochemistry. The frequency of colonies consisting of βIII tubulin-positive neurons, GFAP-positive astrocytes, and O4-positive oligodendrocytes (N, A, O: colonies containing more than 20 positive cells are in capital letters; n, a, o: colonies containing fewer than 19 cells are in lowercase letters) is presented as the percentage of total colonies (50 colonies each) from three independent experiments.

Transfection of CAG-CBRluc-IRES-Venus

To visualize transplanted cells by both fluorescence and luminescence, we established an ES cell line that constitutively expresses a click beetle red-emitting luciferase variant (CBR*luc*) [11] and Venus [a yellow fluorescence protein (YFP) mutant] [12] by transfecting a linearized CAG-CBR*luc*-IRES-Venus plasmid (CCV; Fig. 1**A**) into EB3 ES cells using lipofectamine2000 (Invitrogen). Stably transfected ES cells were selected by G418 (200 μg/ml), subcloned, and screened by the expression of both CBR*luc* and Venus. The Venus could be detected by antibodies against EGFP.

Flow Cytometry

Undifferentiated ES cells, PNS, and SNS were dissociated and processed for flow cytometric analysis by FACS Calibur (Becton-Dickinson). The Venus-positive cells were counted and are presented as the percentage of the total number of cells, excluding dead cells stained by propidium iodide.

Spinal Cord Injury Model and Transplantation

Adult female C57BL/6J mice (20–22 g) were anesthetized via intraperitoneal (i.p.) injection of ketamine (100 mg/kg) and xylazine (10 mg/kg). After laminectomy at the 10th thoracic spinal vertebra (T10), a contusive SCI was induced at the same level using a commercially available SCI device (IH impactor, Precision Systems and Instrumentation, Lexington, KY), as described previously [49]. This device creates a reliable contusion injury by rapidly applying a force-defined impact (60 kdyn) with a stainless steel-tipped impounder. The initial touch point of the impactor with the dura was determined (using the vibrator mode of the impactor tip), and from there a 1.5-mm displacement was applied to the spinal cord. Force curve readings revealed an average value of 63 ± 0.5 kdyn.

Nine days after the injury, CCV-PNS (n = 11) or -SNS (n = 11) that had been cultured for 7 days were partially dissociated and transplanted into the lesion epicenter using a glass micropipette (5×10^5 cells/mouse) and stereotaxic injector (KDS 310, Muromachi-kikai, Tokyo, Japan). An equal volume of PBS was injected into the control group (n = 11). Hind limb motor function was evaluated for 6 weeks after SCI using the locomotor rating test of the Basso-Mouse-Scale (BMS), as described previously [21]. Well-trained investigators, blinded to the treatments, performed the behavioral analysis, determining the BMS scores at the same time each day. All animal experiments were approved by the ethics committee of Keio University, and were in accordance with the Guide for the Care and Use of Laboratory Animals (National Institutes of Health, Bethesda, MD).

Bioluminescence Imaging (BLI)

BLI was performed using a Xenogen-IVIS 100 cooled CCD optical macroscopic imaging system (SC BioScience, Tokyo, Japan) [3,50]. To examine the effective expression of CBR*luc in vitro*, we used a CCD-based macroscope detector to determine the luminescence intensity of cultures with various numbers of cells (0 to 5×10^5 cells per well) in the presence of D-luciferin (150 μg/ml). The integration time was fixed at a 5-min duration for each image, and the signals were reported as photons/cells/sec. For *in vivo* BLI, D-luciferin was injected i.p. into mice (150 mg/kg body weight), and serial images were acquired 15–40 min. later, until a maximum signal intensity was obtained with the field-of-view, which was set at 15 cm. We found this time window to be optimal, since the signal intensity peaked 15–40 min after D-luciferin administration, and was followed by a 15-min plateau (data not shown). All images were analyzed with Igor (WaveMetrics, Lake Oswego, OR) and Living Image software (Xenogen, Alameda, CA), and the optical signal intensity was expressed as photon flux, in units of photons/sec/cm^2/steradian. The results were displayed as a pseudocolor photon count image superimposed on a grayscale anatomic image. To quantify the measured light, we defined a region of interest (ROI) over the cell-implanted area and examined all the values within the same ROI. The signal intensity of the engrafted cells was measured weekly for 6 weeks after transplantation.

Histological Analyses

Animals were anesthetized and transcardially perfused with 4% paraformaldehyde in 0.1 M PBS 6 weeks after transplantation. The spinal cords were removed, embedded in OCT compound (Sakura Finetechnical Co., Ltd.), and sectioned in the sagittal/axial plane at 20 μm on a cryostat (Leica CM3050 S). The injured spinal cords from the three groups were histologically evaluated by Hematoxylin-eosin (H-E) staining, Luxol Fast Blue (LFB) staining, and immunohistochemistry. The injured spinal cord from the vehicle control group 2 weeks after SCI was also evaluated by LFB staining and immunohistochemistry for 5-HT. Both cultured cells and tissue sections were stained with the following primary antibodies: anti-GFP (rabbit IgG, 1:500, MBL), anti-βIII tubulin (mouse IgG, 1:1000, Sigma), Alexa488-conjugated anti-βIII tubulin (mouse IgG, 1:4000, Covance), anti-Hu (human IgG,

1:1000, a gift from Dr. Robert Darnell, The Rockefeller University), anti-GFAP (rabbit IgG, 1:4000, Dako), anti-GFAP (guinea pig IgG, 1:4000, Advanced Immunochemical Inc.), anti-GFAP (rat IgG, 1:200, Invitrogen), anti-O4 (mouse IgM; 1:5000, Chemicon), anti-APC CC-1 (mouse IgG, 1:100, Calbiochem), anti-MBP (chicken IgY, 1:200, Aves Labs), anti-Neurofilament RT97 (NF-H, mouse IgG, 1:200, Chemicon), anti-5-HT (goat IgG, 1:200, Immunostar), anti-GAP43 (mouse IgG, 1:2000, Chemicon), Cy3-conjugated anti-SMA (mouse IgG 1:500, Sigma), anti-PECAM-1 (rat IgG, 1:50, BD Bioscience Pharmingen), and anti-VEGF (rabbit IgG, 1:50, Santa Cruz Biotechnology).

For immunohistochemistry with anti-Venus, VEGF, -NF-H, -5-HT, and -GAP43 antibodies, we used a biotinylated secondary antibody (Jackson Immunoresearch Laboratory, Inc.), after exposure to 0.3% H_2O_2 for 30 minutes at room temperature to inactivate endogenous peroxidase. The signals were enhanced with the Vectastain ABC kit (Vector Laboratories, Inc.). Nuclei were stained with Hoechst33258 (10 μg/ml, Sigma). The samples were examined with a universal fluorescence microscope (Axiocam, Carl Zeiss) or a confocal laser scanning microscope (LSM510, Carl Zeiss).

For immunoelectron microscopy, frozen sections were incubated with nanogold-conjugated anti-rabbit secondary antibody (1:100 Invitrogen) followed by incubation with the primary anti-GFP antibody. After enhancement with HQ-Silver kit (Nanoprobes Inc.), sections were postfixed with 0.5% osmium tetroxide, dehydrated through ethanol, and embedded in Epon. Ultrathin sections were stained with uranyl acetate and lead citrate, observed under a transmission EM (JEOL model 1230), and photographed with a Digital Micrograph 3.3 (Gatan Inc.).

Quantitative Analyses of Stained Tissue Sections through Transplanted Spinal Cord

To quantify HE-, LFB-, or immunostained sections, images were obtained by a universal fluorescence microscope (Axiocam, Carl Zeiss), manually outlined, and quantified by Micro Computer Imaging Device (MCID; Imaging Research Inc., St. Catharines, Ontario, Canada). Constant threshold values were maintained for all the analyses with MCID. HE-stained images were taken at the lesion epicenter and 2, 1, and 0.5 mm rostral and caudal to the epicenter in axial sections at ×25 magnification (n = 5, each). To analyze the LFB-positive area after transplantation, we automatically captured four regions from each animal in axial sections at the lesion epicenter and 2 mm and 1 mm rostral and caudal to the epicenter at ×200 magnification. Analyses were performed 2 weeks or 6 weeks after SCI for the vehicle-control group and 6 weeks after for the PNS and SNS groups. The total myelinated area was quantified by MCID using light intensity gain counting (n = 3, each). For the Venus (GFP)-positive area after transplantation, we captured in midsagittal sections the epicenter at ×25 magnification from each animal (6 weeks after SCI for the vehicle-control, PNS, and SNS groups), and quantified the total Venus-positive area (n = 6, each). NF-H-stained images were taken at the epicenter and 4, 3, 2, 1, and 0.5 mm rostral and caudal to the epicenter in axial sections at ×50 magnification, and the NF-H-positive areas were quantified using light intensity gain counting (n = 5, each). VEGF-stained images were taken at the lesion epicenter in axial sections at ×50, and the VEGF-positive areas were quantified using light intensity gain counting (n = 3, each). To analyze the 5-HT-positive area after transplantation, we automatically captured five regions from each animal in axial sections 4-mm caudal to the lesion epicenter (Th10 level), which was approximately at the L1 level, a non-lesion site, at ×200 magnification. The analysis was performed 2 weeks or 6 weeks after SCI for the vehicle-control group and 6 weeks after for the PNS and SNS groups. The total 5-HT-positive area was quantified (n = 3, for each condition). For the GAP43-positive area after transplantation, we captured the ventral regions in midsagittal sections 1 mm caudal to the epicenter at ×200 magnification from each animal (6 weeks after SCI for the vehicle-control, PNS, and SNS groups), and quantified the total GAP43-positive area (n = 4). To quantify the proportion of cells positive for each cell type-specific marker *in vivo*, we selected representative midsagittal sections and automatically captured five regions within 500 μm rostral and caudal to the lesion epicenter at ×200. The engrafted cells in each section that were positive for both Venus and each cell type-specific marker were counted (n = 4). The PECAM-1-positive blood vessels were counted manually in axial sections of the lesion epicenter at ×200 magnification (n = 3, each).

Statistical Analysis

All data are presented as the mean ± s.e.m. An unpaired two-tailed Student's *t*-test was used for the BLI analyses and Venus-stained analysis, and *in vivo* differentiation assays. ANOVA followed by the Turkey-Kramer test for multiple comparisons among the three transplantation groups was used for the *in vivo* differentiation analysis and PECAM-1-, VEGF-, 5HT-, and GAP43-stained analysis. Repeated measures two-way ANOVA followed by the Turkey-Kramer test was used for HE-, LFB-, NF-H-stained and BMS analysis. Pearson's correlation coefficient was used for correlation of the results of BLI analysis and the quantification of Venus-positive area. In all statistical analyses, the significance was set at $P<0.05$.

Acknowledgments

We thank Drs. H. J. Okano, K. Ishii, W. Akamatsu, S. Ishii, K. Miura, T. Nagai, S. Miyao, and T. Harada for technical assistance and scientific discussion, and all the members of Dr. Okano's laboratory for encouragement and kind support. We thank Drs. Y. Ishibashi, E. Tsuda, T. Yokoyama, and A. Ono for encouragement and kind support. We also thank Dr. H. Niwa for the EB3 cells.

Author Contributions

Conceived and designed the experiments: GK YO YT MN HO. Performed the experiments: GK YO JY NN KK MM OT KF HK SS. Analyzed the data: GK MN. Contributed reagents/materials/analysis tools: GK YO SO SS YM ST MN HO. Wrote the paper: GK YO HK MN HO.

References

1. Ogawa Y, Sawamoto K, Miyata T, Miyao S, Watanabe M, et al. (2002) Transplantation of in vitro-expanded fetal neural progenitor cells results in neurogenesis and functional recovery after spinal cord contusion injury in adult rats. J Neurosci Res 69: 925–933.
2. Iwanami A, Kaneko S, Nakamura M, Kanemura Y, Mori H, et al. (2005) Transplantation of human neural stem cells for spinal cord injury in primates. J Neurosci Res 80: 182–190.
3. Okada S, Ishii K, Yamane J, Iwanami A, Ikegami T, et al. (2005) In vivo imaging of engrafted neural stem cells: its application in evaluating the optimal timing of transplantation for spinal cord injury. Faseb J 19: 1839–1841.
4. Hofstetter CP, Holmstrom NA, Lilja JA, Schweinhardt P, Hao J, et al. (2005) Allodynia limits the usefulness of intraspinal neural stem cell grafts; directed differentiation improves outcome. Nat Neurosci 8: 346–353.
5. Cummings BJ, Uchida N, Tamaki SJ, Salazar DL, Hooshmand M, et al. (2005) Human neural stem cells differentiate and promote locomotor recovery in spinal cord-injured mice. Proc Natl Acad Sci U S A 102: 14069–14074.
6. Bibel M, Richter J, Schrenk K, Tucker KL, Staiger V, et al. (2004) Differentiation of mouse embryonic stem cells into a defined neuronal lineage. Nat Neurosci 7: 1003–1009.

7. McDonald JW, Liu XZ, Qu Y, Liu S, Mickey SK, et al. (1999) Transplanted embryonic stem cells survive, differentiate and promote recovery in injured rat spinal cord. Nat Med 5: 1410–1412.
8. Keirstead HS, Nistor G, Bernal G, Totoiu M, Cloutier F, et al. (2005) Human embryonic stem cell-derived oligodendrocyte progenitor cell transplants remyelinate and restore locomotion after spinal cord injury. J Neurosci 25: 4694–4705.
9. Okada Y, Shimazaki T, Sobue G, Okano H (2004) Retinoic-acid-concentration-dependent acquisition of neural cell identity during in vitro differentiation of mouse embryonic stem cells. Dev Biol 275: 124–142.
10. Okada Y, Matsumoto A, Shimazaki T, Enoki R, Koizumi A, et al. (2008) Spatio-Temporal Recapitulation of Central Nervous System Development By Murine ES Cell-Derived Neural Stem/Progenitor Cells. Stem Cells.
11. Zhao H, Doyle TC, Coquoz O, Kalish F, Rice BW, et al. (2005) Emission spectra of bioluminescent reporters and interaction with mammalian tissue determine the sensitivity of detection in vivo. J Biomed Opt 10: 41210.
12. Nagai T, Ibata K, Park ES, Kubota M, Mikoshiba K, et al. (2002) A variant of yellow fluorescent protein with fast and efficient maturation for cell-biological applications. Nat Biotechnol 20: 87–90.
13. Niwa H, Miyazaki J, Smith AG (2000) Quantitative expression of Oct-3/4 defines differentiation, dedifferentiation or self-renewal of ES cells. Nat Genet 24: 372–376.
14. Wang X, Rosol M, Ge S, Peterson D, McNamara G, et al. (2003) Dynamic tracking of human hematopoietic stem cell engraftment using in vivo bioluminescence imaging. Blood 102: 3478–3482.
15. Contag CH, Bachmann MH (2002) Advances in in vivo bioluminescence imaging of gene expression. Annu Rev Biomed Eng 4: 235–260.
16. Bregman BS (1987) Spinal cord transplants permit the growth of serotonergic axons across the site of neonatal spinal cord transection. Brain Res 431: 265–279.
17. Saruhashi Y, Young W, Perkins R (1996) The recovery of 5-HT immunoreactivity in lumbosacral spinal cord and locomotor function after thoracic hemisection. Exp Neurol 139: 203–213.
18. Ramon-Cueto A, Plant GW, Avila J, Bunge MB (1998) Long-distance axonal regeneration in the transected adult rat spinal cord is promoted by olfactory ensheathing glia transplants. J Neurosci 18: 3803–3815.
19. Kaneko S, Iwanami A, Nakamura M, Kishino A, Kikuchi K, et al. (2006) A selective Sema3A inhibitor enhances regenerative responses and functional recovery of the injured spinal cord. Nat Med 12: 1380–1389.
20. Kobayashi NR, Fan DP, Giehl KM, Bedard AM, Wiegand SJ, et al. (1997) BDNF and NT-4/5 prevent atrophy of rat rubrospinal neurons after cervical axotomy, stimulate GAP-43 and Talpha1-tubulin mRNA expression, and promote axonal regeneration. J Neurosci 17: 9583–9595.
21. Basso DM, Fisher LC, Anderson AJ, Jakeman LB, McTigue DM, et al. (2006) Basso Mouse Scale for locomotion detects differences in recovery after spinal cord injury in five common mouse strains. J Neurotrauma 23: 635–659.
22. Coutts M, Keirstead HS (2007) Stem cells for the treatment of spinal cord injury. Exp Neurol.
23. Temple S (2001) The development of neural stem cells. Nature 414: 112–117.
24. Fan G, Martinowich K, Chin MH, He F, Fouse SD, et al. (2005) DNA methylation controls the timing of astrogliogenesis through regulation of JAK-STAT signaling. Development 132: 3345–3356.
25. Shimozaki K, Namihira M, Nakashima K, Taga T (2005) Stage- and site-specific DNA demethylation during neural cell development from embryonic stem cells. J Neurochem 93: 432–439.
26. Takizawa T, Nakashima K, Namihira M, Ochiai W, Uemura A, et al. (2001) DNA methylation is a critical cell-intrinsic determinant of astrocyte differentiation in the fetal brain. Dev Cell 1: 749–758.
27. Winkler C, Fricker RA, Gates MA, Olsson M, Hammang JP, et al. (1998) Incorporation and glial differentiation of mouse EGF-responsive neural progenitor cells after transplantation into the embryonic rat brain. Mol Cell Neurosci 11: 99–116.
28. Hofstetter CP, Schwarz EJ, Hess D, Widenfalk J, El Manira A, et al. (2002) Marrow stromal cells form guiding strands in the injured spinal cord and promote recovery. Proc Natl Acad Sci U S A 99: 2199–2204.
29. Hill CE, Proschel C, Noble M, Mayer-Proschel M, Gensel JC, et al. (2004) Acute transplantation of glial-restricted precursor cells into spinal cord contusion injuries: survival, differentiation, and effects on lesion environment and axonal regeneration. Exp Neurol 190: 289–310.
30. Cao Q, Xu XM, Devries WH, Enzmann GU, Ping P, et al. (2005) Functional recovery in traumatic spinal cord injury after transplantation of multineurotrophin-expressing glial-restricted precursor cells. J Neurosci 25: 6947–6957.
31. Davies JE, Huang C, Proschel C, Noble M, Mayer-Proschel M, et al. (2006) Astrocytes derived from glial-restricted precursors promote spinal cord repair. J Biol 5: 7.
32. Baehr M, Bunge RP (1990) Growth of adult rat retinal ganglion cell neurites on astrocytes. Glia 3: 293–300.
33. Noble M, Fok-Seang J, Cohen J (1984) Glia are a unique substrate for the in vitro growth of central nervous system neurons. J Neurosci 4: 1892–1903.
34. Tang X, Davies JE, Davies SJ (2003) Changes in distribution, cell associations, and protein expression levels of NG2, neurocan, phosphacan, brevican, versican V2, and tenascin-C during acute to chronic maturation of spinal cord scar tissue. J Neurosci Res 71: 427–444.
35. Bundesen LQ, Scheel TA, Bregman BS, Kromer LF (2003) Ephrin-B2 and EphB2 regulation of astrocyte-meningeal fibroblast interactions in response to spinal cord lesions in adult rats. J Neurosci 23: 7789–7800.
36. De Winter F, Oudega M, Lankhorst AJ, Hamers FP, Blits B, et al. (2002) Injury-induced class 3 semaphorin expression in the rat spinal cord. Exp Neurol 175: 61–75.
37. Moreau-Fauvarque C, Kumanogoh A, Camand E, Jaillard C, Barbin G, et al. (2003) The transmembrane semaphorin Sema4D/CD100, an inhibitor of axonal growth, is expressed on oligodendrocytes and upregulated after CNS lesion. J Neurosci 23: 9229–9239.
38. Berry M, Maxwell WL, Logan A, Mathewson A, McConnell P, et al. (1983) Deposition of scar tissue in the central nervous system. Acta Neurochir Suppl (Wien) 32: 31–53.
39. Okada S, Nakamura M, Katoh H, Miyao T, Shimazaki T, et al. (2006) Conditional ablation of Stat3 or Socs3 discloses a dual role for reactive astrocytes after spinal cord injury. Nat Med 12: 829–834.
40. Buffo A, Rite I, Tripathi P, Lepier A, Colak D, et al. (2008) Origin and progeny of reactive gliosis: A source of multipotent cells in the injured brain. Proc Natl Acad Sci U S A 105: 3581–3586.
41. Blondel O, Collin C, McCarran WJ, Zhu S, Zamostiano R, et al. (2000) A glia-derived signal regulating neuronal differentiation. J Neurosci 20: 8012–8020.
42. Gallo V, Bertolotto A (1990) Extracellular matrix of cultured glial cells: selective expression of chondroitin 4-sulfate by type-2 astrocytes and their progenitors. Exp Cell Res 187: 211–223.
43. Nakamura M, Houghtling RA, MacArthur L, Bayer BM, Bregman BS (2003) Differences in cytokine gene expression profile between acute and secondary injury in adult rat spinal cord. Exp Neurol 184: 313–325.
44. Beattie MS, Bresnahan JC, Komon J, Tovar CA, Van Meter M, et al. (1997) Endogenous repair after spinal cord contusion injuries in the rat. Exp Neurol 148: 453–463.
45. Mense SM, Sengupta A, Zhou M, Lan C, Bentsman G, et al. (2006) Gene expression profiling reveals the profound upregulation of hypoxia-responsive genes in primary human astrocytes. Physiol Genomics 25: 435–449.
46. Yoshida H, Imaizumi T, Tanji K, Matsumiya T, Sakaki H, et al. (2002) Platelet-activating factor enhances the expression of vascular endothelial growth factor in normal human astrocytes. Brain Res 944: 65–72.
47. Liu S, Qu Y, Stewart TJ, Howard MJ, Chakrabortty S, et al. (2000) Embryonic stem cells differentiate into oligodendrocytes and myelinate in culture and after spinal cord transplantation. Proc Natl Acad Sci U S A 97: 6126–6131.
48. Hooper M, Hardy K, Handyside A, Hunter S, Monk M (1987) HPRT-deficient (Lesch-Nyhan) mouse embryos derived from germline colonization by cultured cells. Nature 326: 292–295.
49. Scheff SW, Rabchevsky AG, Fugaccia I, Main JA, Lumpp JE, Jr. (2003) Experimental modeling of spinal cord injury: characterization of a force-defined injury device. J Neurotrauma 20: 179–193.
50. Rice BW, Cable MD, Nelson MB (2001) In vivo imaging of light-emitting probes. J Biomed Opt 6: 432–440.

Therapeutic potential of appropriately evaluated safe-induced pluripotent stem cells for spinal cord injury

Osahiko Tsuji[a,b,1], Kyoko Miura[a,c,1], Yohei Okada[a,d], Kanehiro Fujiyoshi[a,b], Masahiko Mukaino[a,e], Narihito Nagoshi[a,b,f], Kazuya Kitamura[a,b], Gentaro Kumagai[a,g], Makoto Nishino[a], Shuta Tomisato[a], Hisanobu Higashi[a], Toshihiro Nagai[h], Hiroyuki Katoh[a,b,f], Kazuhisa Kohda[a], Yumi Matsuzaki[a], Michisuke Yuzaki[a], Eiji Ikeda[i,j], Yoshiaki Toyama[b], Masaya Nakamura[b,2], Shinya Yamanaka[c], and Hideyuki Okano[a,2]

Departments of [a]Physiology and [b]Orthopedic Surgery, School of Medicine, Keio University, Shinjuku, Tokyo 160-8582, Japan; [c]Center for Induced Pluripotent Stem Cell Research and Application, Kyoto University, Kyoto 606-8507, Japan; [d]Kanrinmaru-Project and Departments of [e]Rehabilitation Medicine, [h]Electron Microscope Laboratory, and [i]Pathology, School of Medicine, Keio University, Tokyo 160-8582, Japan; [f]Department of Orthopedic Surgery, National Hospital Organization, Murayama Medical Center, Tokyo 208-0011, Japan; [g]Department of Orthopedic Surgery, Graduate School of Medicine, Hirosaki University, Aomori 036-8560, Japan; and [j]Department of Pathology, Graduate School of Medicine, Yamaguchi University, Yamaguchi 755-8505, Japan

Edited by Fred Gage, Salk Institute, San Diego, CA, and approved June 3, 2010 (received for review September 3, 2009)

Various types of induced pluripotent stem (iPS) cells have been established by different methods, and each type exhibits different biological properties. Before iPS cell-based clinical applications can be initiated, detailed evaluations of the cells, including their differentiation potentials and tumorigenic activities in different contexts, should be investigated to establish their safety and effectiveness for cell transplantation therapies. Here we show the directed neural differentiation of murine iPS cells and examine their therapeutic potential in a mouse spinal cord injury (SCI) model. "Safe" iPS-derived neurospheres, which had been pre-evaluated as nontumorigenic by their transplantation into nonobese diabetic/severe combined immunodeficiency (NOD/SCID) mouse brain, produced electrophysiologically functional neurons, astrocytes, and oligodendrocytes in vitro. Furthermore, when the safe iPS-derived neurospheres were transplanted into the spinal cord 9 d after contusive injury, they differentiated into all three neural lineages without forming teratomas or other tumors. They also participated in remyelination and induced the axonal regrowth of host 5HT$^+$ serotonergic fibers, promoting locomotor function recovery. However, the transplantation of iPS-derived neurospheres pre-evaluated as "unsafe" showed robust teratoma formation and sudden locomotor functional loss after functional recovery in the SCI model. These findings suggest that pre-evaluated safe iPS clone-derived neural stem/progenitor cells may be a promising cell source for transplantation therapy for SCI.

neural stem/progenitor cell | cell transplantation | regenerative medicine | remyelination | axonal regrowth

Given their ability to generate all types of neural cells, neural stem/progenitor cells (NS/PCs) are a promising source for cell replacement therapy for various intractable CNS disorders (reviewed in refs. 1–6). Notably, ES cells have great developmental plasticity and can be induced to become NS/PCs with specific differentiation potentials (7–11), making them a major candidate for cell replacement therapies for CNS disorders (12–16). The clinical use of ES cells is complicated, however, by ethical and immunological concerns, both of which might be overcome by using pluripotent stem cells derived directly from a patient's own somatic cells (17).

We recently reported the establishment of induced pluripotent stem (iPS) cells from mouse fibroblasts by the retroviral introduction of four factors (*Oct3/4*, *Sox2*, *Klf4*, and *c-Myc*) with selection for *Fbxo15* expression (18) and *Nanog* expression (19, 20). Compared with *Fbxo15*-selected iPS cells, *Nanog*-selected iPS cells more closely resembled ES cells' gene-expression pattern and could contribute to germline-competent adult chimeras (19–21). More recently, we and others (22, 23) generated iPS cells without using *c-Myc* retroviruses, albeit with lower efficiency. The successful establishment of these iPS cell lines, along with initial reports showing efficacy in the therapeutic use of iPS cells in rodent models of sickle cell anemia (24) and Parkinson disease (25), led us to examine the use of iPS cells as a treatment for spinal cord injury (SCI).

A number of important issues need to be addressed before a clinical trial using iPS cells as a cell-therapy source for SCI is initiated. First, a detailed evaluation of iPS cells' potential to generate neural cells compared with ES cells is required. Second, iPS cells are likely to carry a higher risk of tumorigenicity than ES cells, due to the inappropriate reprogramming of these somatic cells, the activation of exogenous transcription factors, or other reasons (25–27). Thus, it is essential to confirm the safety of grafted iPS-derived NS/PCs. Finally, the effectiveness of iPS-derived NS/PC transplantation as a treatment for SCI must be evaluated.

In the previous study, we pre-evaluated iPS clones for safety by transplanting iPS-derived neurospheres into the NOD/SCID mouse brain (27). Here, we show that the transplantation of neurospheres derived from safe iPS cell clones into the injured spinal cord promoted functional recovery without any tumor formation. In contrast, the transplantation of neurospheres derived from unsafe iPS cells, showing robust teratoma formation in the NOD/SCID mouse brain, also resulted in initial functional recovery, but was later followed by teratoma formation and deterioration of locomotor function. These data suggest that the evaluation of in vitro differentiation and in vivo tumorigenicity are important for identifying safe iPS clones for cell therapy, and that the NS/PCs derived from iPS clones deemed safe by such pre-evaluation are a promising source for cell therapy for SCI.

Results

Pre-Evaluated Safe MEF-iPS Cells Exhibit ES-Like Neural Differentiation Potentials in Vitro. We previously reported the neural differentiation of 36 independent murine iPS cell clones (27). The results of this study led us to classify several iPS clones as safe or unsafe

Author contributions: O.T., K.M., M. Nakamura, S.Y., and H.O. designed research; O.T., K.M., Y.O., K.F., M.M., N.N., K. Kitamura, G.K., M. Nishino, S.T., H.H., T.N., H.K., E.I., and H.O. performed research; O.T. and K.M. contributed new reagents/analytic tools; O.T., K.M., Y.O., K.F., M.M., N.N., K. Kitamura, G.K., H.K., K. Kohda, Y.M., M.Y., E.I., Y.T., M. Nakamura, S.Y., and H.O. analyzed data; and O.T., K.M., Y.O., K.F., H.K., E.I., M. Nakamura, and H.O. wrote the paper.

The authors declare no conflict of interest.

This article is a PNAS Direct Submission.

[1]O.T. and K.M. contributed equally to this work.

[2]To whom correspondence may be addressed. E-mail: hidokano@sc.itc.keio.ac.jp or masa@sc.itc.keio.ac.jp.

This article contains supporting information online at www.pnas.org/lookup/suppl/doi:10.1073/pnas.0910106107/-/DCSupplemental.

clones, according to the teratoma-forming activity of the iPS-derived neurospheres after transplantation into the NOD/SCID mouse brain.

Here, we first performed a detailed examination of the neural differentiation potential of a safe iPS clone, 38C2, which was established from mouse embryonic fibroblasts (MEFs) by the introduction of four factors, including *c-Myc*, and by the selection for *Nanog* expression (19, 28), and compared them with mouse ES cells (EB3) (29, 30). 38C2 iPS cells and EB3 ES cells were induced into embryoid bodies (EBs) in medium containing a low concentration of retinoic acid, then dissociated and cultured in suspension in serum-free medium with FGF-2 for 7 or 8 d to form primary neurospheres (PNS) (38C2 iPS/EB3 ES-PNS) (29). These PNSs were dissociated and formed secondary neurospheres (38C2 iPS/EB3 ES-SNS) under the same conditions (Fig. 1*A*). To induce further differentiation, 38C2 iPS-SNSs were adherently cultured in the absence of FGF-2, resulting in the generation of Tuj1$^+$ neurons (4.9 ± 0.8%), GFAP$^+$ astrocytes (11.3 ± 1.2%), and CNPase$^+$ oligodendrocytes (3.7 ± 0.9%), as well as Nestin$^+$ neural progenitor cells (25.9 ± 6.5%; Fig. 1 *B* and *C*), suggesting that 38C2 iPS-SNS have similar differentiation potentials to EB3 ES-SNS. The 38C2 iPS-PNSs could also generate TH$^+$ catecholaminergic, 5HT$^+$ serotonergic, and GAD67$^+$ GABAergic neurons (Fig. S1). RT-PCR analysis of the expression of cell-type-specific markers in the progeny of the 38C2 iPS cells showed drastic decrease of the expression of undifferentiated ES cell marker genes, such as *Nanog*, *Eras*, and *Oct3/4*, and the up-regulation of neural markers such as *Sox1*, *βIII-tubulin*, and *GFAP* during the neural differentiation of 38C2 iPS cells, similar to EB3 ES cells (Fig. 1*D*).

Moreover, electrophysiological analysis using whole-cell patch clamping in both the 38C2 iPS-PNS– and EB ES-PNS–derived neurons after 21–28 d of adherent differentiation showed tetrodotoxin (TTX; 1 μM)-sensitive repetitive action potentials in the current-clamp mode [38C2 iPS-PNS (n = 11 of 16) and EB3 ES-PNS (n = 5 of 7)] (Fig. S2*A*) and very rapid inward currents immediately followed by transient outward currents in voltage-clamp mode (Fig. S2*B* 1 and 2). Steady outward currents, similar to those mediated by delayed-rectifier K$^+$ channels, were also observed (Fig. S2 *B*1 and *D*). These findings suggest that 38C2 iPS-PNSs produced neuronal cells equipped with functional channels that could generate and modify action potentials (*SI Text*).

Safe MEF-iPS Cells Can Differentiate into Trilineage Neural Cells in the Injured Spinal Cord Without Tumorigenesis. Previously, we confirmed that SNSs from the safe 38C2 MEF-iPS cell clone survived and showed no teratoma-forming activity in the NOD/SCID mouse brain for 24 wk after transplantation (27) (Fig. S3). 38C2 iPS-SNSs that were transplanted into the intact spinal cord survived and differentiated into trilineage neural cells without any tumorigenesis (Fig. S4). Next, to evaluate their therapeutic effects in the mouse SCI model, we transplanted 38C2 iPS-SNSs into the contused spinal cord 9 d after injury and compared them with EB3 ES-SNSs, using adult fibroblasts and PBS as controls. We also made a comparison with 38C2 iPS-PNSs, because we recently confirmed that the transplantation of ES cell-derived SNSs, but not PNSs, provides therapeutic benefit after SCI (31). We transplanted 38C2 iPS-SNSs that had been prelabeled by lentivirus to express both CBR*luc* and mRFP (32, 33) into the lesion epicenter 9 d after the injury. Bioluminescence imaging (BLI) analysis (34), which detects luciferase photon signals only from living cells, revealed an approximate graft survival rate of 18% at 35 d after transplantation (Fig. 2*A*). We also histologically confirmed that the grafted cells survived and exhibited no apparent evidence of tumorigenesis (Fig. 2*B*), and that there were no Nanog$^+$ cells (Fig. S5), at least during our observation

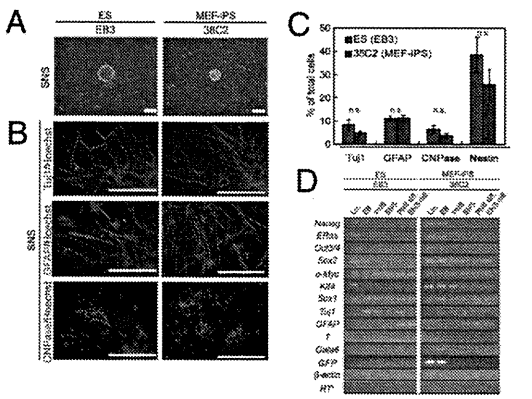

Fig. 1. Neural differentiation of pre-evaluated safe MEF-iPS cells in vitro. (*A*) Neurospheres derived from EB3 ES cells and 38C2 iPS cells. (Scale bar: 200 μm.) (*B*) Immunocytochemical analysis of neural cell marker proteins in the differentiated SNSs derived from EB3 ES and 38C2 iPS cells. (Scale bar: 100 μm.) (*C*) Neural differentiation efficiencies of neurospheres derived from EB3 ES and 38C2 iPS cells. (n = 5, n.s.). (*D*) RT-PCR analysis of undifferentiated cells (Un.), EBs, PNSs, SNSs, differentiated PNSs (PNS diff.), and SNSs (SNS diff.) of the EB3-ES and 38C2 iPS cells.

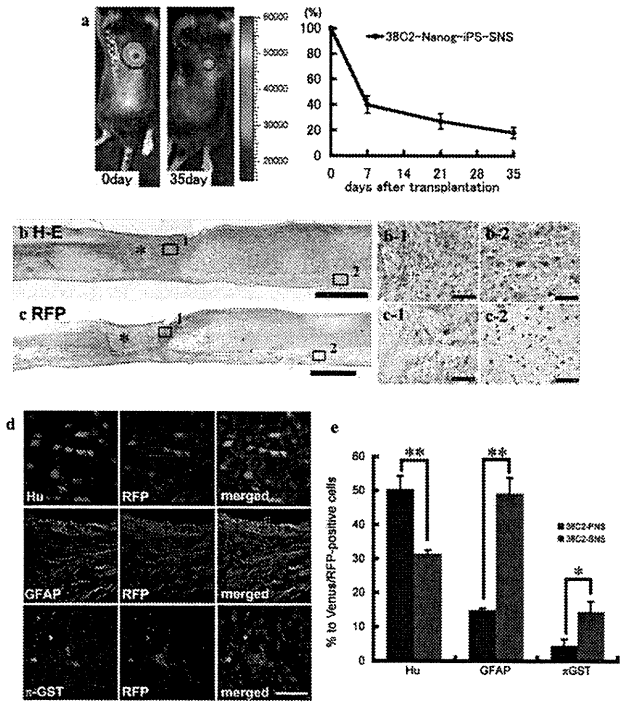

Fig. 2. Transplanted SNSs derived from safe MEF-iPS clones survive without any evidence of tumorigenesis and differentiate into trilineage neural cells in the injured spinal cord. (*A*) Representative BLI images of a mouse in which CBR*luc*-expressing 38C2 iPS-SNSs were transplanted into the injured spinal cord (*Left*, immediately after transplantation; *Right*, 42 d after transplantation). Quantification of the photon intensity revealed that ≈60% of the grafted cells were lost within 7 d after transplantation, and ≈20% of the cells survived 35 d after transplantation. Values are means ± SEM (n = 6). (*B*) H&E and (*C*) anti-RFP DAB staining of sagittal sections of the spinal cord 42 d after injury (38C2 iPS-SNS transplanted). There was no evidence of tumorigenesis (*B*). No significant nuclear atypia was observed in magnified images of the boxed areas showing the lesion epicenter (*B*-1) or white matter caudal to the transplantation site (*B*-2). Grafted cells survived and were diffusely distributed rostral and caudal to the lesion site (*C*). Higher-magnification images of the boxed areas showing the lesion site (*C*-1) and white matter caudal to the lesion site (*C*-2). *Lesion epicenter. (*D*) Immunohistochemical analyses of 38C2 iPS-SNSs grafted into spinal cord 42 d after injury, revealing grafted cells double-positive for RFP and markers of neural lineages. (*E*) Quantitative analyses of Hu$^+$ neurons, GFAP$^+$ astrocytes, and π-GST$^+$ oligodendrocytes. Values are means ± SEM (n = 3 each; *P < 0.05, **P < 0.01).

period. Grafted RFP$^+$ cells were located mainly around the lesion epicenter, whereas some cells had migrated as far as 4 mm rostral and caudal to the graft site (Fig. 2*C*). In the injured spinal cord, the grafted 38C2 iPS-SNSs differentiated into three types of neural cells, including Hu$^+$ neurons (31.4 ± 1.1%), GFAP$^+$ astrocytes (49.3 ± 4.5%), and π-GST$^+$ oligodendrocytes (14.4 ± 3.0%), whereas 38C2 iPS-PNSs differentiated dominantly into neurons—that is, Hu$^+$ neurons (50.4 ± 3.8%), GFAP$^+$ astrocytes (14.9 ± 0.6%), and π-GST$^+$ oligodendrocytes (4.6 ± 1.8%) (Fig. 2 *D* and *E* and Fig. S6).

Transplantation of SNSs Derived from Safe MEF-iPS Cells into the Injured Spinal Cord Promotes Functional Recovery. The contusive SCI initially caused complete paralysis, followed by gradual recovery that reached a plateau. There were statistically significant differences in Basso mouse scale (BMS) between the 38C2 iPS-SNS and PBS groups at 21, 28, 35, and 42 d after injury, whereas no significant difference was observed between the 38C2 iPS-SNS and EB3 ES-SNS groups. Forty-two days after injury, the 38C2 iPS-SNS–grafted animals could lift their trunks and had significantly better BMS than the PBS control or adult fibroblast-treated animals, which were unable to support their body weight with their hindlimbs (Fig. 3*A*). To reveal the potential mechanism of functional recovery after 38C2 iPS-SNS transplantation, we conducted further histological analyses. By Luxol Fast Blue (LFB) staining, 38C2 iPS-SNS–grafted mice showed a significantly larger myelinated area at the lesion epicenter than the PBS control mice at 42 d after injury (Fig. 3*B*). We also found that grafted 38C2 iPS-SNS–derived cells myelinated NF200$^+$ host neuronal fibers, confirmed by the positive staining of RFP and myelin basic protein (MBP; Fig. 3*C*), indicating that graft cell-derived oligodendrocytes were capable of remyelination. For further confirmation of the myelinating ability of 38C2 iPS-SNSs, we transplanted 38C2 iPS-SNSs into the injured spinal cord of MBP-null *shiverer* mice, a severely hypo- and dysmyelinating mutant mouse that lacks the major dense line of CNS myelin (35). Myelinating potential of the grafted 38C2 iPS-SNS–derived cells was confirmed, exhibiting MBP$^+$ deposits (Fig. 3*D*) and the major dense line, by electron microscopic analysis (Fig. 3*E*).

To determine the effect of the grafted 38C2 iPS-SNSs on serotonergic nerve fibers, which are important for the motor functional recovery of hind limbs (36, 37), we immunostained for 5HT and quantified the positive area at the distal cord 1, 2, and 6 wk after injury. Some of the nerve fibers associated with graft cell-derived Hu$^+$ neurons were identified as 5HT$^+$ serotonergic fibers, and were prominent at the distal cord compared with the PBS control group (Fig. 4 *A–C*). Quantitative analysis of the serotonergic innervation of the distal cord revealed a significant difference between the 38C2 iPS-SNS and PBS control groups (Fig. 4*B*). The contusive injury (60 kDyn) resulted in a significant decrease in the number of 5HT$^+$ fibers at the distal cord, followed by a slight recovery, which is the nature of contusive SCI. The injection of PBS in the PBS control group did not induce any additional increase in the number of 5HT$^+$ fibers at the distal cord. In contrast, innervation of the distal cord by these 5HT$^+$ fibers was enhanced by the grafted 38C2 iPS-SNS 6 wk after SCI (Fig. 4*B*). Moreover, 38C2 iPS-SNS–derived astrocytes, which exhibited a bipolar morphology with long processes, were observed closely associated with the 5HT$^+$ serotonergic fibers (Fig. 4*D*).

Transplantation of Neurospheres Derived from Pre-Evaluated Safe or Unsafe TTF-iPS Cells into the Injured Spinal Cord. Toward the goal of clinical application, we next examined the therapeutic potential

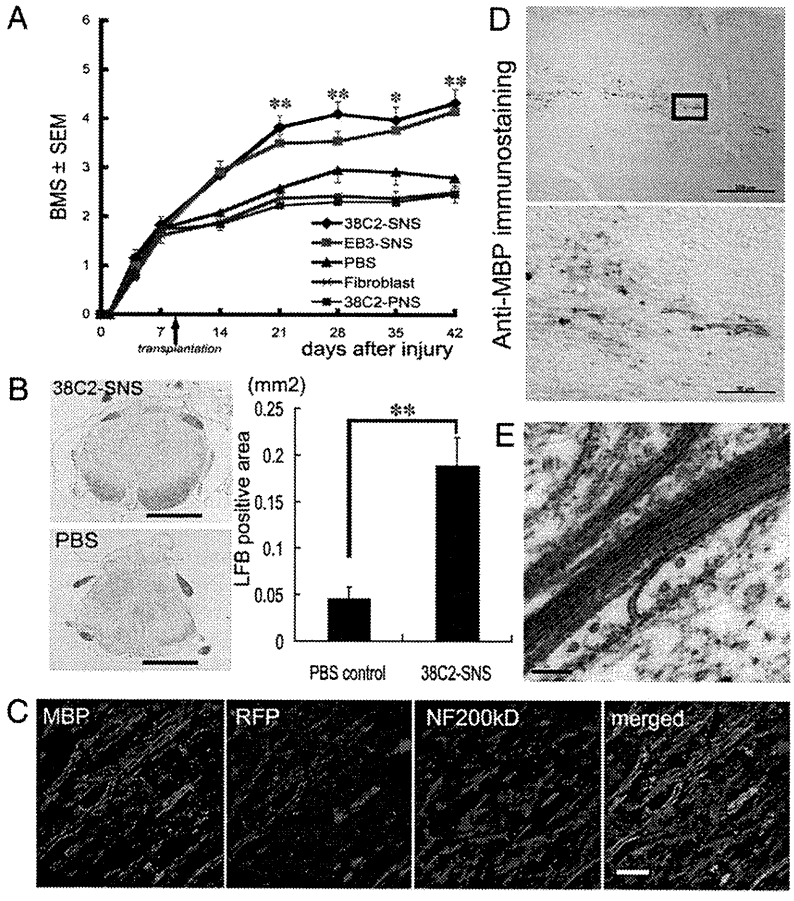

Fig. 3. SNS derived from a safe MEF-iPS clone differentiate into mature oligodendrocytes and promote remyelination. (*A*) Time course of functional recovery of hind limbs evaluated by BMS. 38C2 iPS-SNS, $n = 19$; EB3 ES-SNS, $n = 15$; PBS, $n = 12$; adult fibroblasts, $n = 13$; 38C2 iPS-PNS, $n = 13$. $^*P < 0.05$, $^{**}P < 0.01$. (*B*) LFB staining of axial sections of the spinal cord at the lesion epicenter 42 d after injury; 38C2 iPS-SNS–transplanted (*Upper Left*) and PBS control (*Lower Left*) animals. Quantification of LFB-positive areas at the lesion epicenter 42 d after injury (*Right*, $n = 7$ each; $^{**}P < 0.01$). (*C*) Immunohistochemistry of 38C2 iPS-SNS–derived mature oligodendrocytes (MBP$^+$). Grafted cells were integrated into myelin sheath. (*D*) Anti-MBP DAB staining of sagittally sectioned spinal cord of a *shiverer* mouse 8 wk after transplantation. MBP$^+$ myelin was detected in the area caudal to the lesion epicenter. (*Lower*) Higher-magnification image of the boxed area. (*E*) EM pictures of the injured spinal cord of a 38C2 iPS-SNS–grafted *shiverer* mouse exhibiting a prominent major dense line and intraperiod lines in multiple compacted lamellae. (Scale bars: *B*, 500 μm; *D Upper*, 200 μm; *C* and *D Lower*, 50 μm; and *E*, 0.1 μm.)

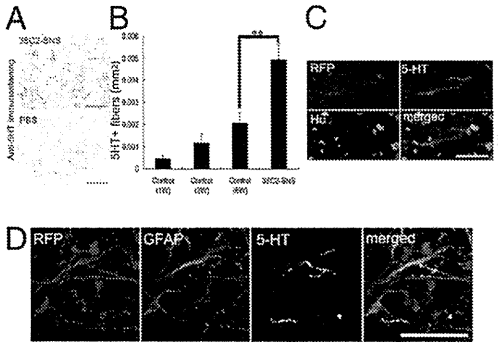

Fig. 4. SNSs derived from a safe MEF-iPS clone promote serotonergic innervation of the dorsal cord and result in better functional recovery of the hindlimbs. (*A*) 38C2 iPS-SNS transplantation promoted the growth of 5HT$^+$ serotonergic fibers in the distal spinal cord. Axial sections of 38C2 iPS-SNS–transplanted (*Upper*) and PBS control mice (*Lower*). (*B*) Quantitative analysis of 5HT$^+$ serotonergic fibers of distal cord in the PBS control (1, 2, and 6 wk postinjury) and 38C2 iPS-SNS transplantation groups (6 wk postinjury; 1 and 2 wk postinjury, $n = 3$ each; 6 wk postinjury and 38C2 SNS, $n = 7$ each; $^{**}P < 0.01$). (*C* and *D*) Immunohistochemistry of 38C2 iPS-SNS–derived neurons (*C*, RFP$^+$, Hu$^+$) and astrocytes (*D*, RFP$^+$, GFAP$^+$) closely associated with 5HT$^+$ serotonergic fibers. (Scale bars: *A*, 100 μm; *C*, 20 μm; *D*, 50 μm.)

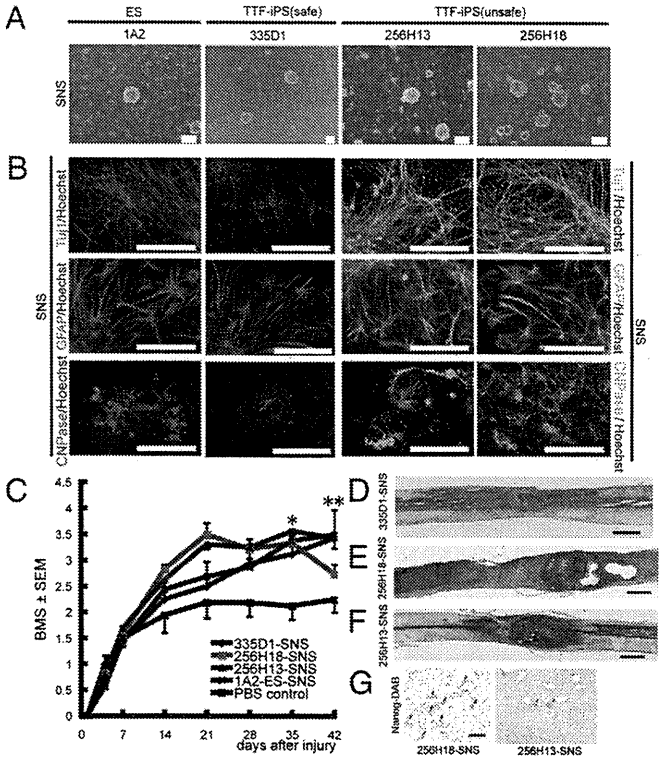

Fig. 5. Characterization and transplantation of SNSs derived from safe and unsafe TTF-iPS cells. (*A*) Neurospheres derived from 1A2 ES cells, 335D1, 256H13, and 256H18 iPS cells. (Scale bar: 200 μm.) (*B*) The differentiation potential of TTF-iPS-derived SNSs tested in vitro by immunocytochemical analyses of neural cell markers; Tuj1 for neurons, GFAP for astrocytes, and CNPase for oligodendrocytes. (Scale bar: 100 μm.) (*C*) Time course of functional recovery of the hindlimbs evaluated by BMS. 335D1 iPS-SNS: $n = 9$ each; 256H13 and 256H18 iPS-SNS: $n = 9$; 1A2 ES-SNS: $n = 9$; PBS control: $n = 8$. $^*P < 0.05$, $^{**}P < 0.01$. (*D–F*) H&E sagittal sections of the spinal cord 42 d after injury. (*D*) 335D1 iPS-SNS, (*E*) 256H18 iPS-SNS, and (*F*) 256H13 iPS-SNS grafted mice. There was no evidence of tumorigenesis in the 335D1 iPS-SNS grafted mice (*D*), whereas teratoma formation was detected within the injured spinal cord in both 256H18 iPS-SNS (*E*), and 256H13 iPS-SNS (*F*) grafted mice. (*G*) Anti-Nanog DAB staining of sagittally sectioned spinal cord of 256H18 and 256H13 iPS-SNS–transplanted animals 35 d after transplantation.

of adult tissue-derived iPS cells. Among six TTF-iPS clones pre-evaluated in our previous study (27), we used the safe 335D1 TTF-iPS clone, which was generated with *Nanog* selection and without the transduction of c-Myc. We also used the unsafe 256H13 and 256H18 TTF-iPS clones (22, 27), which were generated without genetic selection or the transduction of c-Myc, and were originally established from CAG-EGFP mice (22). A subclone of RF8 ES cells carrying the *Nanog*-EGFP reporter (1A2) (19) was used as control. All of the TTF-iPS clones formed PNSs and SNSs (Fig. 5*A*), and generated cells of all three neural lineages, similar to those derived from 1A2 ES cells (Fig. 5*B*). We transplanted these TTF-iPS–derived SNSs into injured spinal cords 9 d after injury. Transplantation of the safe 335D1 iPS-SNS (prelabeled with RFP lentivirally) resulted in better functional recovery compared with the PBS control group, without any apparent tumorigenesis during our observation period (Fig. 5 *C* and *D*). Grafted and survived RFP$^+$ 335D1 iPS-SNS–derived cells could differentiate into neural trilineages (Fig. S7 *A* and *B*). Furthermore, LFB staining revealed that 335D1 iPS-SNS–grafted mice had a significantly larger myelinated area at the lesion epicenter than the PBS control mice at 42 d after injury (Fig. S8 *A* and *B*), and grafted RFP$^+$ 335D1 SNS-derived cells differentiated into MBP$^+$ oligodendrocytes (Fig. S8*C*). However, all unsafe 256H18 iPS-SNS–grafted mice and one of 256H13 iPS-SNS–grafted mice formed teratomas containing EGFP$^+$ donor cells within the injured spinal cord (Fig. 5 *E* and *F* and Fig. S7*C*). Histological analyses revealed that these teratomas contained epithelial and smooth muscle tissue (Fig. S9*A*), and also exhibited Nanog immunoreactivity (Fig. 5*G*). Although the motor functions gradually recovered in both groups to the same extent as in the safe 335D1 iPS-SNS recipients until 35 d after injury, the 256H18 iPS-SNS–grafted animals exhibited a sudden deterioration of motor function 42 d after injury. In contrast, the 256H13 iPS-SNS–grafted animals maintained their functional recovery at 42 d after injury (Fig. 5*C*). Notably, in most mice of the 256H13 iPS-SNS group, scattered small clusters of Nanog$^+$ cells were observed in the spinal cords without obvious teratoma formation (Fig. S9 *B* and *C*). Thus, we speculate that teratoma formation and subsequent deterioration of function recovery would occur in the 256H13 group if a longer observation period was set.

Discussion

In the present study, we showed that the pre-evaluated safe iPS cells could produce neurospheres containing NS/PCs (Fig. 1*A*) that give rise to trilineage neural cells, including several types of neurons (Fig. 1 *B* and *C*), and that the neurons were electrophysiologically functional in vitro similar to ES cells (Fig. S2).

Based on these safety assessments and in vitro findings, we performed an in vivo study using the safe 38C2 MEF-iPS cell clone. Grafted 38C2 iPS-SNSs differentiated into neurons, astrocytes, and oligodendrocytes without forming teratomas or other tumors, and promoted functional recovery after SCI, whereas 38C2 iPS-PNSs did not show any therapeutic effects (Fig. 3*A*). These findings were compatible with our recent data on mouse ES cell-derived neurosphere transplantation into an identical mouse SCI model (31). Transplantation of ES-derived SNSs, which can differentiate into neural trilineages, promoted remyelination, axonal regrowth and tissue sparing, leading to improved function. In contrast, predominantly neurogenic PNSs showed no therapeutic effects on SCI (31). Thus, we elected to use iPS-SNSs and not iPS-PNSs for this study. In fact, the grafted 38C2 iPS-SNSs formed MBP$^+$ myelin sheaths within the injured spinal cord. We also confirmed the myelination potential of 38C2 iPS-SNS–derived cells in the spinal cord of the MBP-null *shiverer* mouse by electron microscopy (Fig. 3

D and *E*). These findings suggested the possibility of the remyelination of demyelinated axons by the grafted 38C2 iPS-SNS–derived oligodendrocytes, which may have contributed to the functional recovery of the grafted animals.

Another potential mechanism for functional recovery is axonal regrowth supported by iPS-SNS–derived astrocytes. Here, we observed grafted 38C2 iPS-SNS–derived $GFAP^+$ astrocytes, which exhibited a bipolar morphology with long processes extending along the axis of the spinal cord, caudal to the lesion epicenter, in close association with $5HT^+$ host serotonergic fibers (Fig. 4*D*). A previous report indicated that immature astrocytes derived from cells grafted into the injured spinal cord promote the outgrowth of $5HT^+$ fibers by offering a growth-permissive surface (38). Consistent with this finding, the transplantation of 38C2 iPS-SNSs promoted serotonergic innervation of the distal cord compared with the PBS control animals, thereby enhancing functional recovery after SCI (Fig. 4 *A* and *B*) (36). Furthermore, trophic factors, such as neurotrophin-3 (NT-3) and brain-derived neurotrophic factor (BDNF), were expressed in 38C2 iPS-SNSs, which could act as an integral part of the observed functional recovery (39, 40). The tissue sparing (e.g., neuroprotection, axon sprouting and remyelination) and other effects, including functional remodeling of spinal locomotor circuits (41), of trophic factors secreted from grafted cells are considered to be important for functional recovery (42). Thus, the combined effects of the 38C2 iPS-SNS–derived glial cells probably contributed to locomotor function recovery.

For clinical applications, the findings with TTF-iPS cells were promising, as most SCI patients are adults. The transplantation of SNSs derived from a pre-evaluated safe TTF-iPS clone promoted functional recovery after SCI without teratoma formation, like the SNSs from safe MEF-iPS clone did (Fig. 5*D*). However, the transplantation of SNSs derived from the unsafe TTF-iPS cells resulted in teratoma formation and functional deterioration. The teratoma-forming activity of TTF-iPS-SNSs could be caused by the presence of undifferentiated cells that might be resistant to differentiation signals within the SNSs (27). In fact, we recently reported that persistent presence of undifferentiated cells within iPS-SNSs highly correlated with teratoma-forming propensity, assayed by flow cytometric analysis using *Nanog*-EGFP reporter and transplantation into the brains of immunodeficient (NOD/SCID) (27). Before iPS cells of adult origin can be used clinically, important hurdles must still be overcome. Though new methods for establishing iPS cells are constantly being developed, including virus-free (43) and transgene-free (44) systems, a new strategy is needed to exclude undifferentiated cells from the differentiated progeny of iPS cells. These findings show that the pre-evaluation of iPS cells' in vitro differentiation potential could play a critical role in terms of their safety and therapeutic effects on the mouse SCI model. Thus, iPS-derived neurosphere transplantation has potential therapeutic use in SCI, when the iPS cell clones are carefully pre-evaluated.

From a clinical viewpoint, it is particularly encouraging that delaying the iPS-derived NS/PC transplantation (to 9 d after injury) enhanced both the survival of the grafted cells and functional recovery, the therapeutic effects of which is almost comparable to those of fetal CNS-derived NS/PCs transplantation (refs. 34 and 45). This finding may also be applicable to the treatment of patients with SCI. Since our first report of iPS cells (18), there has been increasing interest in their characteristics and therapeutic potential. Our present study demonstrates the therapeutic potential of iPS-derived NS/PCs for SCI repair. Before any clinical trial of human CNS disorders using iPS cells, it will be essential to pre-evaluate each iPS cell clone carefully to guarantee a safety level equal to other types of cells, such as Schwann cells (46, 47) and fetal-derived neurosphere cells (NS/PCs) (3), and to conduct preclinical transplantation studies using appropriate primate models (48, 49).

Methods

Reverse-Transcription and RT-PCR. RNA was isolated with TRIzol (Invitrogen) according to the manufacturer's instructions. Total RNA (0.5 μg) was treated with TURBO DNase (Ambion) and then reverse-transcribed with oligo (dT) primer and SuperScript III (Invitrogen). The primers and PCR conditions used in this study are listed Table S1.

Cell Culture, Neural Induction, and Immunocytochemistry. Mouse ES and iPS cells were cultured as described previously (19, 28, 29). Mouse ES and iPS cells were differentiated into neurospheres via EBs treated with 10^{-8} M retinoic acid (Sigma), as described previously with minor modification (28, 29). (Detailed differentiation protocol is described in *SI Text*.) ES and iPS cell-derived neurospheres were dissociated and differentiated on poly-L-ornithine/fibronectin-coated coverslips for 5 d and subjected to immunocytochemical analysis. The number of cells immunoreactive for each marker was counted and shown as the percentage of the total number of cells counterstained with Hoechst 33258. The antibodies used in this study are listed in Table S2.

Lentivirus Production and Infection of Secondary Neurospheres. For BLI tracing of grafted 38C2 iPS-SNSs, we generated a modified lentivirus vector encoding both the click beetle red luciferase (CBR*luc*; Promega) and mRFP, pCSII-EF-CBR*luc*-IRES2-mRFP (32, 33). For lentivirus preparation, HEK-293T cells were transfected with pCSII-EF-CBR*luc*-IRES2-mRFP, pCAG-HIVgp, and pCMV-VSV-G-RSV-Rev, and the conditioned medium containing virus particles was concentrated and used for viral transduction.

Spinal Cord Injury Model and Transplantation. Adult female C57BL/6J mice (20–22 g) were anesthetized via an i.p. injection of ketamine (100 mg/kg) and xylazine (10 mg/kg). A contusive spinal cord injury using an Infinite Horizon Impactor (60 kdyn; Precision Systems) was induced at the Th10 level as reported previously (34). For transplantation, 5×10^5 cells of mouse ES/iPS cell-derived neurospheres, adult dermal fibroblasts in 2 μL of cell suspension, or PBS was injected into the lesion epicenter. Hindlimb motor function was evaluated by the locomotor rating of the Basso mouse scale (BMS) (50) for 42 d after injury. For the in vivo imaging of intact and injured spinal cords after the transplantation, a Xenogen-IVIS 100 cooled CCD optical macroscopic imaging system (SC BioScience) was used for BLI, as reported previously (34) (*SI Text*). All procedures were approved by the ethics committee of Keio University, and were in accordance with the Guide for the Care and Use of Laboratory Animals (National Institutes of Health). Grafted animals were deeply anesthetized and intracardially perfused with 4% paraformaldehyde (PFA; pH 7.4). The dissected spinal cords were sectioned into 20-μm axial/sagittal sections using a cryostat and processed for histological analyses. Detailed conditions for histological analyses are described in *SI Text*.

Statistical Analysis. All data are reported as the mean ± SEM. An unpaired two-tailed Student's *t* test was used for the analyses of in vitro and in vivo 38C2 iPS-SNS and ES-SNS differentiation efficiency (Figs. 1*C* and 2*E*), $5HT^+$ areas (Fig. 4*B*), and LFB^+ areas (Fig. 2*B*). Repeated-measures two-way ANOVA, followed by the Tukey–Kramer test, was used for BMS analysis. $^*P < 0.05$, $^{**}P < 0.01$.

ACKNOWLEDGMENTS. We thank Drs. H. Abe, T. Sunabori, F. Renault-Mihara, W. Akamatsu, S. Shibata, T. Harada, S. Miyao, and H. J. Okano (Keio University) for technical assistance and scientific discussions, and all the members of Dr. Okano's and Dr. Yamanaka's laboratories for encouragement and generous support. We also thank Drs. K. Okita, M. Koyanagi, and K. Tanabe (Kyoto University) for the undifferentiated iPS cells, Dr. H. Niwa (Riken CDB) for the EB3 ES cells, Dr. R. Farese (University of California-San Francisco) for the RF8 ES cells, Dr. R. Y. Tsien (University of California-San Diego) for the mRFP gene, Dr. A. Miyawaki (Riken BSI) for the Venus gene, Dr. H. Baba (Tokyo University of Phamacy and Life Science) for the shiverer mice, and Dr. H. Miyoshi (Riken BRC) for the lentiviral vectors. We especially thank Drs. S. Okada (Kyusyu University), A. Iwanami (University of California-San Francisco and Keio University), and J. Yamane (Keio University) for scientific discussions, technical advice, and encouragement. This work was supported by grants from the Program for Promotion of Fundamental Studies in Health Sciences of the National Institute of Biomedical Innovation (NIBIO), a grant from Uehara Memorial Foundation, and Grants-in-Aid for Scientific Research from the Japan Society for the Promotion of Science (JSPS) and the Ministry of Education, Culture, Sports, Science and Technology of Japan (MEXT), the project for realization of regenerative medicine and support for the core institutes for iPS cell research from MEXT; Japan Science and Technology Agency (SORST); the Ministry of Health, Labor, and Welfare; the General Insurance Association of Japan; Research Fellowships for Young Scientists from the Japan Society for the Promotion of Science; Keio Gijuku Academic Development Funds; and a Grant-in-aid for the Global COE program from MEXT to Keio University.